Hydrothermal solubility of Dy hydroxide as a function of pH and stability of Dy hydroxyl aqueous complexes from 25 to 250 °C

Sarah E. Smith-Schmitz [a,*], Alexander P. Gysi [a,b]

[a] New Mexico Bureau of Geology and Mineral Resources, New Mexico Institute of Mining and Technology, Socorro, NM 87801, USA

[b] Department of Earth and Environment Science, New Mexico Institute of Mining and Technology, Socorro, NM 87801, USA

[*] Corresponding author: Email address: sarah.smith@nmt.edu

REVISION 2

ABSTRACT

The rare earth elements (REE) have important applications in green energy technologies. The formation of mineral deposits in geologic systems commonly involves hydrothermal fluids which can mobilize the REE. However, the REE speciation is not well known as a function of pH. The thermodynamic properties of REE hydroxyl complexes used in geochemical models are based on the Helgeson-Kirkham-Flowers (HKF) equation of state parameters which were derived by extrapolation of low temperature experimental and estimated data. In this study, Dy hydroxide solubility experiments are combined with available literature data to improve these models from 25 to 250 °C and optimize the thermodynamic properties of Dy^{3+} and Dy hydroxyl complexes using GEMSFITS. Batch-type solubility experiments were conducted from 150 to 250 °C and at saturated water vapor pressure in perchloric acid solutions with initial pH values of 2 to 5 in 0.5 pH unit increments. The measured solubility of Dy hydroxide is retrograde with temperature and decreases with pH. The logarithm of total dissolved Dy molality ranges from -2.3 to -5.3 at 150 °C (pH 4.7-5.5), from -2.4 to -5.6 at 200 °C (pH 3.9-5.1), and from -3.7 to -6.9 at 250 °C (pH of 3.4 and 5.0). The optimized standard partial molal Gibbs energies of formation ($\Delta_f G°_T$) derived for Dy^{3+} and $DyOH^{2+}$ display a close to linear relationship with temperature, fitting with previous optimizations based on $DyPO_4$ solubility data in the literature. A comparison of the optimized $\Delta_f G°_T$ values for aqueous Dy species with predictions from available HKF parameters indicates significant differences ranging from +11 to -26 kJ/mol between 25 and 250 °C. The experimental fits are used to derive the Dy hydroxide solubility products (K_{s0}) and formation constants for the hydrolysis of Dy (β_n with n = 1 to 3; $Dy^{3+} + n OH^- = DyOH_n^{3-n}$) as a function of temperature. The optimization method presented yields accurate thermodynamic properties for the Dy^{3+} aqua ions and the $DyOH^{2+}$ species at the acidic to mildly acidic pH studied whereas more experimental work is needed at near-neutral and alkaline conditions to better constrain the other hydroxyl complexes.

The optimized thermodynamic data have a significant impact on geochemical modeling of the mobility and solubility of REE minerals in acidic hydrothermal fluids.

Keywords: Dysprosium, hydrolysis, solubility experiments, thermodynamics, hydrothermal, rare earth elements, hydroxides

Highlights:

- The solubility of Dy hydroxide was measured in acidic to mildly acidic perchloric acid solutions from 150 to 250 °C.
- Thermodynamic data for Dy^{3+} and Dy hydroxyl species were optimized using solubility data from this study and the literature.
- The optimized data deviate by up to -26 kJ/mol from values predicted using available HKF equation of state parameters.
- Dy hydroxide solubility and Dy^{3+} hydrolysis constants are derived from 25-250 °C based on the optimized data.
- The updated data have significant implications for geochemical modeling of heavy REE mobility in acidic hydrothermal fluids.

1. INTRODUCTION

The rare earth elements (REE) are economically important due to their numerous applications in the high-tech and green energy industries (Watari et al., 2020). Hydrothermal aqueous fluids are known to play an important role in the formation of REE mineral deposits (e.g. Gysi et al., 2016; Migdisov et al., 2016; Patel et al., 2023). Experimental studies have shown that chloride (Cl^-) and sulfate (SO_4^{2-}) are important ligands controlling the mobilization of REE in acidic hydrothermal fluids (Louvel et al., 2015; Migdisov et al., 2016; Wan et al., 2021; Guan et al., 2022a, 2022b). Fluoride (F^-) is considered a possible depositional ligand due to the insoluble nature of F-bearing REE minerals such bastnäsite (Migdisov and Williams-Jones, 2014; Migdisov et al., 2016). The REE hydroxyl and carbonate complexes can potentially become important transporting ligands with increased pH as predicted from geochemical modeling (Perry and Gysi, 2018) and recent experimental work (Louvel et al., 2022; Nisbet et al., 2022). However, the accuracy of these models is unknown due to a lack of available high temperature experimental data for these species as a function of pH (Migdisov et al., 2016; Pan et al., 2024).

Thermodynamic properties of REE hydroxyl aqueous complexes used for geochemical modeling are primarily based on the work by Haas et al. (1995). Their study provides a set of Helgeson-Kirkham-Flowers (HKF) equation of state parameters (Helgeson et al., 1981; Shock and Helgeson, 1988; Tanger and Helgeson, 1988; Shock et al., 1992) to predict the stability of REE species in hydrothermal fluids. The HKF parameters for the REE^{3+} aqua ions are commonly taken from Shock and Helgeson (1988) and Shock et al. (1997). However, such predicted HKF parameters can be quite inaccurate (see review by Migdisov et al., 2016). Wood et al. (2002) investigated the hydrolysis constants for Nd species (i.e., $NdOH^{2+}$, $Nd(OH)_2^+$, and $Nd(OH)_3^0$) between pH 3.4 and 9.5 and at temperatures up to 290 °C using potentiometric experiments. Their study indicates that the Nd^{3+} aqua ion should be more stable than predicted from the HKF

parameters derived by Haas et al. (1995). Furthermore, hydrothermal monazite and xenotime solubility experiments conducted in acidic solutions between 100 and 250 °C (Gysi et al., 2018; Gysi and Harlov, 2021) indicate that the HKF parameters for the the REE^{3+} aqua ion and $REEOH^{+2}$ species result in significant (up to 3-4 orders of magnitude) discrepancies in predicted mineral solubilities.

In this study, batch-type Dy hydroxide solubility experiments were conducted in mildly acidic to acidic aqueous solutions and at temperatures from 150 to 250 °C at saturated water vapor pressure. The solubility data are combined with literature values for the solubility of $DyPO_4$ to optimize the thermodynamic properties of Dy^{3+} aqua ion and Dy hydroxyl complexes between 25 and 250 °C using the thermodynamic optimization program GEMSFITS (Miron et al., 2015). The experimentally derived standard partial molal Gibbs energies permit deriving a set of equilibrium constants that more accurately predict the hydrolysis of Dy in hydrothermal fluids. These data are implemented in the MINES database (Gysi et al., 2023) to simulate the mobility of Dy at hydrothermal conditions.

2. METHODS

2.1. Materials

Synthesis of Dy hydroxide powders is based on the method described by Diakonov et al. (1998a). Pure Dy_2O_3 (Alfa Aesar, REacton^{TM} grade, 99.99% pure) was first mixed with MilliQ water (18.2 MΩ·cm) which was then added to a Teflon-lined Parr 4744 acid digestion vessel. The headspace of the reactor was purged with research grade N_2 gas for 5 minutes prior to hydrothermal synthesis. The vessel was then sealed and placed in a muffle furnace and the solution was equilibrated at 250 °C for up to 21 days. At the end of the synthesis procedure, the reactor was quenched in a water bath, the Dy hydroxide powder collected, dried, weighed, and stored in a sealed polypropylene

vial in a desiccator. These synthetic Dy hydroxide powders were characterized for crystallinity and purity using powder X-ray diffraction (XRD) and Raman spectroscopy (Fig. 1). The refined crystal lattice parameters are listed in Table 1. The Raman spectra for Dy hydroxide exhibit peaks at 313, 399, and 502 cm^{-1} (Supplementary Materials, Table S1) corresponding to Raman vibrational modes of the Dy hydroxide crystalline lattice and a strong peak at ~3600 cm^{-1} corresponding to the O-H stretching mode (Zeng et al., 2010; Cui and Hope, 2015; Sanivarapu et al., 2018; Hurtig et al., 2024). The Raman spectra of post-experimental Dy hydroxide powders also lacks any carbonate peak (near ~1090 cm^{-1}) confirming the purity of the solids used in the experiments.

The perchloric acid based experimental starting solutions (pH of 2 to 5) were prepared by titrating perchloric acid (Fisher Scientific, trace metal grade) into MilliQ water. The initial pH of these experimental starting solutions ($pH_{init.,25°C}$) was measured using a 913 Metrohm pH meter (accuracy of ± 0.003) equipped with a pH electrode (Metrohm, unitrode 6.0260. 020) calibrated using 1.68, 4.01, and 7.00 Fisher buffer solutions (accuracy of ±0.01). These pH values were then used to determine the molality of perchlorate (ClO_4^-) in the experimental starting solutions. Perchloric acid was chosen because ClO_4^- does not form detectable complexes with REE at concentrations of less than ~6 mol/L (Choppin et al., 1966; Migdisov and Williams-Jones, 2002).

2.2. Experimental Methods

Batch-type $Dy(OH)_3(s)$ solubility experiments were carried out in 45 ml Teflon-lined stainless steel reactors (Parr Instruments Company, 4744; Fig. 2) using perchloric acid based experimental starting solutions with initial pH values of 2 to 5 in 0.5 pH unit increments. The experimental solutions were equilibrated for up to 24 days with $Dy(OH)_3(s)$ powders at temperatures of 150, 200, and 250 °C and at saturated water vapor pressure. Kinetic experiments were carried out for

durations between 1 and 24 days and replicate experiments were conducted to determine the experimental uncertainty.

A typical experiment consists of first loading ~40 mg synthetic $Dy(OH)_3(s)$ powder in each of the virgin grade Teflon sample holders which are sealed with a porous Teflon membrane; this set up provides a kinetic barrier to avoid any possible back reaction upon quenching of the reactors (Loges et al., 2013). The sample holders are then each loaded into a reactor Teflon-liner with 25 ml of the chosen perchloric acid based experimental starting solution; the headspace of each reactor is purged for ~5 minutes with research grade N_2 gas. The vessels are then sealed and placed in a muffle furnace (ColeParmer®, EW-33858–80) and maintained within ± 1 °C. The temperature is monitored using an Omega® temperature logger attached to a K-type thermocouple inserted into the center of the furnace. At the end of each experiment, the reactors are quenched in less than 20−30 minutes using a cold water bath. The quenched experimental solutions are then collected and filtered through a 0.22 μm membrane syringe filter to remove any particles in suspension prior to acidification. The filtered solutions are collected in polypropylene vials and acidified using nitric acid (Fisher Chemical, trace metal grade) for further analysis of Dy using inductively coupled plasma optical emission spectroscopy (ICP-OES) and inductively coupled plasma mass spectrometry (ICP-MS). After an experiment, the reactor liners are washed with sulfuric acid according to the method delineated in the study by Gysi and Harlov (2021) to determine potential formation of precipitates post quenching. Analysis of these solutions using ICP-MS did not reveal any detectable REE concentrations. The liners were then soaked with concentrated sulfuric acid cleaning solutions, followed by a distilled water soak. To ensure that subsequent experiments were not cross-contaminated, blank experiments were conducted between between experimental runs by addition of the perchloric acid starting solutions to the cleaned vessels which were then heated to the experimental temperatures for a minimum of 2 days.

137

138 *2.3 Analytical Methods*

139 X-ray diffraction analysis was performed using a PANalytical X'Pert Pro diffractometer at the
140 New Mexico Bureau of Geology and Mineral Resources. The $Dy(OH)_3(s)$ powders were scanned
141 using Cu-Kα radiation using 2θ scanning values ranging between 5° and 70° in 0.02° steps. The
142 measured diffractograms were background subtracted, the peaks fitted and matched to the relevant
143 phase identified using the MAUD Rietveld refinement software (Lutterotti et al., 1999).

144 Raman analysis was carried out using a Horiba LabRAM HR Evolution confocal Raman
145 microscope at the New Mexico Bureau of Geology and Mineral Resources. Raman spectra were
146 collected at an excitation laser wavelength of 532 nm using a 1800 groove/mm grating. Data
147 analysis was carried out using Fityk curve and peak fitting open source software (Wojdyr, 2010).

148 Dissolved Dy concentrations above 30 ppb were measured in the quenched experimental
149 solutions in acidified (2% HNO_3 matrix) solutions using an Agilent 5900 ICP-OES instrument at
150 the Analytical Chemistry Laboratory in the New Mexico Bureau of Geology and Mineral
151 Resources. An in-line internal standard containing 10 ppm In (SCP Science, NIST traceable) was
152 used for drift corrections. Analytical standard solutions were prepared by dilution of a multi REE
153 standard (Inorganic Ventures, CMS-1, 10.01 ± 0.04 ppm Dy) with a 2% HNO_3 (trace metal grade,
154 Fisher Chemical) blank matrix solution. The analytical precision (95% confidence level) based on
155 repeated standard analysis was better than 1% for Dy concentrations ranging between 2×10^{-7} and
156 6×10^{-6} mol/kg Dy (33–975 ppb). A limit of detection (LOD) of 1 ppb Dy was determined using
157 repeated analysis (5σ) of the procedural blank.

158 Dissolved Dy concentrations below 30 ppb were analyzed in acidified (2% HNO_3 matrix)
159 quenched experimental solutions using a quadrupole Agilent 7900 solution ICP-MS instrument at
160 the Analytical Chemistry Laboratory in the New Mexico Bureau of Geology and Mineral

Resources. An in-line 50 ppb In standard (SCP Science, NIST traceable) was used as an internal standard for instrumental drift corrections. Samples were analyzed using an in-line He gas collision cell to reduce any interference that can result from REE oxide formation. Analytical standards were prepared from a multi REE standard (Inorganic Ventures, CMS-1, 10.01 ± 0.04 ppm Dy) diluted with a 2% HNO_3 (trace metal grade, Fisher Chemical) blank matrix solutions. The analytical precision (95% confidence level) based on repeated standard analysis is 1 % within a concentrations range between 7.8×10^{-8} and 1.5×10^{-7} mol/kg Dy (13 - 25 ppb). A LOD of 3 ppt Dy was determined from repeated analysis (5σ) of the procedural blank.

3. DATA TREATMENT

3.1. Speciation, pH, and activity calculations

Calculations of aqueous speciation and pH were carried out at the experimental temperatures and at saturated water vapor pressure using GEM-Selektor (Kulik et al., 2013) and GEMSFITS (Miron et al., 2015). Thermodynamic data for the minerals and aqueous species in the Dy-Cl-O-H component system used in these calculations are from the MINES thermodynamic database (Gysi et al., 2023) with data sources used summarized in Table S2. The thermodynamic data used for the aqueous Dy species (Dy^{3+} aqua ion and hydroxyl complexes) were taken from Shock and Helgeson (1988), Haas et al. (1995), and Shock et al. (1997); the thermodynamic data for the remaining aqueous species are from the slop98.dat database originally implemented in the SUPCRT92 program (Johnson et al., 1992). This dataset is hereafter referred to as Supcrt92. The data used for $Dy(OH)_3(s)$ were taken from Diakonov et al. (1998b) with the heat capacity data estimated using the data for $Tb(OH)_3$. The differences in the $\Delta_f G°_T$ values for $Dy(OH)_3(s)$ calculated using the heat capacity data for either $Tb(OH)_3$ or $Ho(OH)_3$ are negligible over the temperature range of this study (less than 0.01%). The data for $Dy_2O_3(s)$ were taken from Morss

and Konings (2004) combined with the heat capacity data from Konings et al. (2014).

The TSolMod library (Wagner et al., 2012) is used in GEMS and GEMSFITS for all of the activity and equation of state (EoS) calculations. The thermodynamic properties of aqueous species were calculated using the revised HKF EoS (Helgeson et al., 1981; Shock and Helgeson, 1988; Tanger and Helgeson, 1988; Shock et al., 1992). The properties of H_2O were calculated using the IAPS-84 EoS (Kestin et al., 1984). The activity coefficients (γ_i) of charged aqueous species were calculated using the extended Debye-Hückel equation (Robinson and Stokes, 1968):

$$log\gamma_i = \frac{-Az_i^2\sqrt{I}}{1+aB\sqrt{I}} + \Gamma_\gamma + b_\gamma I \quad (1)$$

with the ionic strength (I) given by:

$$I = \frac{1}{2}\sum m_i z_i^2 \quad (2)$$

where A and B are the Debye-Hückel parameters from Helgeson et al. (1981); $\mathring{a}_i$ is the ion size parameter taken from Kielland (1937) for charged species with the exception of ClO_4^- (4.5 Å) from Migdisov and Williams-Jones (2007); Γ_γ is a mole fraction to molality conversion factor; $b\gamma$ is the extended term parameter, which has a value of 0.21 for perchloric acid based aqueous solutions up to 250 °C (Migdisov and Williams-Jones, 2007); m_i and z_i are the molal concentration and the charge of the ith aqueous species respectively. The γ_i of water was calculated from the osmotic coefficient (Helgeson et al., 1981), and the γ_i was set to unity for all neutral aqueous species.

The pH was calculated at each experimental temperature from the known molality of ClO_4^- added to the experimental starting solutions and the total dissolved Dy concentrations measured in the quenched experimental solutions. The pH in the experimental solutions at temperature is controlled by both the solubility of Dy hydroxide and the hydrolysis reactions of Dy:

$$Dy(OH)_{3(s)} = Dy^{3+} + 3OH^- \quad (K_{s0}) \quad (3)$$

$$Dy^{3+} + OH^- = DyOH^{2+} \quad (\beta_1) \quad (4)$$

208 $Dy^{3+} + 2OH^- = Dy(OH)_2^+$ (β_2) (5)

209 $Dy^{3+} + 3OH^- = Dy(OH)_3^0$ (β_3) (6)

210 where K_{s0} is the solubility product, and β_1-β_3 are the formation constants of Dy hydroxyl
211 complexes. The predicted equilibrium pH was initially calculated using GEMS and the
212 thermodynamic properties for Dy aqueous species from Supcrt92 (Table S2) to allow comparison
213 of the experimental and predicted Dy hydroxide solubility. These uncorrected pH values, defined
214 here as "$pH_{T,uncorr}$" (Table S3), were re-calculated following optimization of the thermodynamic
215 properties of the Dy^{3+} aqua ion and hydroxyl complexes as described below. The set of calculated
216 equilibrium pH values obtained after optimizations are defined here as "$pH_{T,opt}$" (Table S4).
217
218 *3.2. Gibbs energy optimization calculations*
219 Optimization of the apparent standard partial molal Gibbs energy of formation at temperature
220 ($\Delta_f G°_T$) was conducted using GEMSFITS (Miron et al., 2015). The optimization method is similar
221 to the method described by Gysi et al. (2018) and Gysi and Harlov (2021) for the solubility of REE
222 phosphates and the properties of REE aqueous species. This program is coupled with the GEMS3K
223 chemical solver (Kulik et al., 2013) based on Gibbs energy minimization. The latter is also used
224 in GEMS and therefore the same EoS, thermodynamic data, and activity models described above
225 are used here.
226 The $\Delta_f G°_T$ values of selected aqueous species (i.e. Dy^{3+}, $DyOH^{2+}$, $Dy(OH)_2^+$) are adjusted
227 at each temperature by conducting simultaneous equilibrium speciation, pH, and mineral solubility
228 calculations. The equilibrium speciation and total dissolved Dy concentrations in equilibrium with
229 Dy hydroxide are calculated from the input solution chemistry (Table 2). The computed Dy
230 solubility is then compared to the measured Dy concentrations until GEMSFITS converges the
231 $\Delta_f G°_T$ values of selected aqueous species to best fit the experimental data. The thermodynamic

properties of other REE hydroxyl species ($Dy(OH)_3^0$ and $Dy(OH)_4^-$) are not well constrained in the studied pH range due to their lower calculated activities (Table S3); furthermore, the existence of the $REE(OH)_4^-$ species listed in Haas et al. (1995) has not been identified to at least 290 °C (Wood et al., 2002), and was therefore omitted in the recommended thermodynamic properties derived in our study. Hence, the properties of $Dy(OH)_3^0$ were fixed using reaction constraints based on the equilibrium constants derived from the original fits of Haas et al. (1995). For example, at 250 °C the $\Delta_f G°_T$ value for $Dy(OH)_3^0$ was adjusted based on the optimized $\Delta_f G°_T$ value for $Dy(OH)_2^+$ derived in our study while using a fixed equilibrium constant based on Haas et al. (1995) for the reaction:

$$Dy(OH)_2^+ + H_2O = Dy(OH)_3^0 + H^+ \quad (7)$$

The $DyPO_4$ solubility data from Gysi et al. (2015) at pH 2 and at temperatures between 100 and 250 °C were retrieved from the ThermoExp_REE experimental database (Pan et al., 2024) and combined with the solubility data from this study during optimizations to better constrain the properties of the Dy^{3+} aqua ion in the lower pH range. GEMFITS also outputs fitting statistics, including a composite scaled sensitivity factor (CSS) and correlation factors for each optimized species (Miron et al., 2015). The composite scaled sensitivity factor indicates the sensitivity of the dependent variable (total dissolved Dy) to changes in $\Delta_f G°_T$ for the optimized species; a higher CSS value indicates therefore a higher sensitivity of the fitted species with respect to the experimental solubility data.

4. RESULTS AND DISCUSSION

4.1. Dy hydroxide solubility experiments

Kinetic experiments were conducted from 1 to 24 days to determine approach to equilibrium between the experimental solutions and Dy hydroxide solids. Table 2 lists the measured Dy

compositions of the quenched experimental solutions. Figure 3 shows the total dissolved Dy concentrations as a function of time for experiments conducted at 150 and 250 °C with initial pH of 3.0 and 2.0, respectively. Both experiments indicate approach to steady state dissolved Dy concentrations after ~9−10 days of reaction, which is interpreted to indicate approach to equilibrium for all the experiments conducted for at least 9 days of reaction time.

The solubility of Dy hydroxide is strongly dependent on pH of the experimental starting solutions and retrograde with temperature (Table 2). Figure 4 shows the measured logarithm molality of total dissolved Dy (log (*m*Dy), in mol/kg) as a function temperature and initial pH of the experimental starting solutions ($pH_{init.,25°C}$). The log (*m*Dy) values range from -2.3 to -5.3 at 150 °C, from -2.4 to -5.6 at 200 °C, and from -3.7 to -6.9 at 250 °C, for $pH_{init.,25°C}$ values from 2.0 to 5.0. In the low pH experiments ($pH_{init.,25°C}$ from 2.0 to 3.5) the effect of temperature on Dy hydroxide solubility is minor in the studied temperature range such that for each $pH_{init.,25°C}$ the average log (*m*Dy) values change by less than ~0.2 log unit from 150 to 250 °C. In the higher pH experiments ($pH_{init.,25°C}$ from 4.0 to 5.0), the Dy concentrations decrease more considerably with temperature with log (*m*Dy) values decreasing by 0.5 to 1.6 log units between 150 and 250 °C.

Comparison of the measured and predicted Dy hydroxide solubility curves as a function of temperature and $pH_{init.,25°C}$ (Fig. 4) indicates that the predicted values diverge from the experimental data with increased pH and temperature. The measured log (*m*Dy) values are as much as 0.7 log units higher ($pH_{init.,25°C}$ 5.0) than the predicted values in the 150 °C experiments, 0.7 log units higher ($pH_{init.,25°C}$ 4.5) in the 200 °C experiments, and range from 0.2 to 0.4 log units higher ($pH_{init.,25°C}$ from 3.0 to 4.0) to 0.7 log units lower ($pH_{init.,25°C}$ 5.0) for the 250 °C experiments.

In order to further investigate the discrepancies between the experimental and predicted Dy hydroxide solubility, a series of speciation calculations were carried out in GEMS using the experimental fluid compositions (Table 2) and the thermodynamic properties for aqueous Dy

species from Supcrt92 (Table S2). These calculations give uncorrected *a priori* estimates of the pH values at the experimental temperatures (Table S3, $pH_{T,uncorr}$). This can be recognized by the resulting solubility profile for Dy concentration as a function of pH that are problematic for the experimental data (Fig. S1), i.e. they do not result in the expected "U-shaped curve" or steep negative slope in the acidic to mildly acidic range that should become flatter with increased pH due to the stepwise hydrolysis of a cation (Baes and Mesmer, 1976, 1981). This progressive change in slope is related to the reaction stoichiometry associated with the hydrolysis of Dy (Eqs. 4-6), which controls the calculated pH. These significant discrepancies indicate a need to re-evaluate the thermodynamic properties of the Dy aqueous species that control the hydrolysis of Dy in the studied pH range.

4.2. Thermodynamic parameter optimizations for aqueous Dy species

The apparent standard partial molal Gibbs energies of formation ($\Delta_f G°_T$) were optimized at each experimental temperature using GEMSFITS with the optimization results listed in Table 3 and shown in Figure 5. More detailed results, including calculated pH of the experimental solutions and calculated logarithm molalities for each Dy aqueous species are listed in Table S4. At 100 °C, both Dy^{3+} and $DyOH^{2+}$ are optimized based on the solubility data for $DyPO_4$ from Gysi et al. (2015), whereas the other Dy hydroxyl species must be reaction constrained using the hydrolysis constants by Haas et al. (1995) due to their lower calculated activities; these optimizations result in residuals (calculated vs. measured Dy concentrations) generally better than ~1-3 % (Table S4). At 150, 200, and 250 °C, the $\Delta_f G°_T$ values for Dy^{3+}, $DyOH^{2+}$, and $Dy(OH)_2^+$ are optimized simultaneously to yield a best fit to the Dy hydroxide solubility data derived in this study; residuals are generally better than ~1-5 % (Table S4).

The optimized $\Delta_f G°_T$ values of the different Dy species exhibit systematic linear trends with

temperature between 100 and 250 °C (Fig. 5a) and produce significant corrections for Dy^{3+} in comparison to the predicted $\Delta_f G°_T$ values from Supcrt92; differences range from -21 to -26 kJ/mol between 100 and 250 °C (Table 3; Fig. 5b). These corrections are consistent with the updated $\Delta_f G°$ values at 25 °C derived by Pan et al. (2024) for Dy^{3+} which were calculated based on available hydrothermal solubility data for $DyPO_4$ between 100 and 250 °C. A comparison of the optimized $\Delta_f G°_T$ values derived in our study with the Pan et al. (2024) $\Delta_f G°$ values (Fig. 5a) shows that Dy^{3+} is in excellent agreement with those predictions between 25 and 250 °C. Hence, the approach used by Pan et al. (2024) to correct the Gibbs energy of Dy^{3+} at 25 °C combined with the HKF parameters from Haas et al. (1995), adequately reproduces the optimized $\Delta_f G°_T$ values derived in our study up to 250 °C.

Conversely, the optimization of $\Delta_f G°_T$ values for $DyOH^{2+}$ and other Dy hydroxyl species between 100 and 250 °C indicates significant differences (Fig. 5, Table 3) in comparison to the values derived by combining the HKF parameters from Haas et al. (1995) with the 25 °C $\Delta_f G°$ from Pan et al. (2024). These differences indicate that the HKF parameters derived by Haas et al. (1995) for the Dy hydroxyl complexes do not adequately predict the properties of Dy hydroxyl complexes in the studied temperature range. In turn, the properties for Dy hydroxyl complexes derived in the study by Pan et al. (2024) do not match our experimental data because in their study these properties had to be reaction constrained based on the study of Haas et al. (1995). Nevertheless, the $\Delta_f G°_T$ values at 25 °C derived by Pan et al. (2024) for the Dy hydroxyl species can be fitted reasonably well with the $\Delta_f G°_T$ values derived from our solubility data (Fig. 5) resulting in R^2 values of 0.95-0.99 for both Dy^{3+} and $DyOH^{2+}$ (Table 4); other species display poorer fits with R^2 value of 0.23-0.59 for $Dy(OH)_2^+$ and $Dy(OH)_3^0$.

Although this study covers a higher pH range than in the optimization study by Pan et al. (2024), experimental data are needed at more alkaline conditions to provide more certainty in the

optimization of Gibbs energies for $Dy(OH)_2^+$ and $Dy(OH)_3^0$. In particular, reaction constraints fixed with equilibrium constants derived from Haas et al. (1995) (Table 3) produce some optimization problems such as scattering of the derived $\Delta_f G°_T$ values with temperature reflected by the R^2 values in Table 4. The thermodynamic properties for $Dy(OH)_2^+$ and $Dy(OH)_3^0$ should therefore be viewed as preliminary values to maintain internal consistency with the optimized Dy^{3+} and $DyOH^{2+}$ species which are more confidently predicted at the studied experimental conditions.

4.3. pH and speciation calculations using the optimized properties for Dy species

Aqueous Dy speciation was calculated at the experimental temperature in GEMSFITS using the compositions of the quenched experimental solutions (Table 2) and the optimized thermodynamic properties from Table 3. Plots of Dy solubility and speciation in log molality (Fig. 6) and log activity (Fig. S2) as a function of $pH_{T,opt}$ show that the measured solubility data display two slopes that can be split by pH range. These slopes are controlled by Dy^{3+} (Eq. 2, Fig. S2a with a slope of -3) in the lower pH and the hydrolysis of Dy (Eqs. 3 and 4, Fig. S2c,e with a slope of -2) in the higher pH range. Hence the Dy^{3+} and $DyOH^{+2}$ species generally control the observed solubility trends with pH, which is also shown by the optimized speciation calculations (Fig. 6b,d,f) displaying an increased stability of the $DyOH^{+2}$ species over the Dy^{3+} with increased temperature. The sensitivity of the fitted species (Table S5) indicates that the optimization of both Dy^{3+} and $DyOH^{+2}$ species are necessary in the studied pH range at 150 °C, whereas $Dy(OH)_2^+$ also needs to be optimized at temperatures between 200 and 250 °C to fit the experimental data.

Further inspection of the calculated logarithm molalities of aqueous Dy species versus pH (Fig. 6) indicates that Dy^{3+} controls the solubility of Dy hydroxide at pH between 4.7 and 5.5, with contributions from Dy hydroxyl species above pH 5.2 at 150 °C. With increased temperature, the stability field of the Dy hydroxyl complexes becomes larger and the calculated equilibrium pH

range is lower, with pH values ranging between 3.9 and 5.1 at 200 °C, and between 3.4 and 5.0 at 250 °C. The optimized speciation calculations further indicate that $DyOH^{2+}$ becomes predominant over a wide pH range in the experiments conducted at 250 °C (Fig. 6e,f). These results contrast with the speciation calculations using Supcrt92 (Fig. S1), which over predict the stability of the Dy hydroxyl species relative to the Dy^{3+} aqua ion between pH 2 to ~5.5. In the study by Pan et al. (2024), the optimized thermodynamic properties for the REE phosphates (monazite and xenotime) indicate a similar result for the solubility of heavy REE phosphates, with an increased stability of the heavy REE^{3+} aqua ions over the other REE hydroxyl complexes for a given pH range in comparison to calculations using Supcrt92. A similar observation was made in the study by Wood et al. (2002) for Nd^{3+} vs. Nd hydroxyl complexes, which gives confidence in the speciation behavior derived from our optimization study.

To our knowledge, the study by Wood et al. (2002) and our study are still the only documented studies providing a detailed analysis of REE^{3+} and REE hydroxyl speciation at saturated water vapor pressure and temperatures above 100 to 300 °C based on REE hydroxide solubility experiments. The study by Wood et al. (2002) used *in situ* potentiometry to determine the solubility Nd hydroxide from 30 to 290 °C. The study by Deberdt et al. (1998) investigated the solubility of La and Gd hydroxide and measured the pH of their experimental solutions between 40 and 90 °C, and calculated it at 150 °C using the REE and NH_3 concentrations measured in the quenched fluids. A major assumption in this study was that the REE^{3+} is the only aqueous REE species present in their experiments and controlling total dissolved REE concentrations. However, this assumption is unlikely at pH values up to 6-7 at 150 °C reported in their study. Indeed, a recent UV-Vis spectrophotometric study by Han and Gysi (2024) at 25 °C indicates that the Er^{3+} aqua ion is replaced by Er hydroxyl species at pH of ~7-7.5; this transition to REE hydroxyl species is expected to occur at lower pH with increased temperature. The combined potentiometric and

376 solubility data from Wood et al. (2002) for Nd and Deberdt et al. (1998) for La and Gd suggest
377 that the light REE^{3+} species is predominant at pH values up to 7-8 from 90 to 100 °C and up to a
378 pH values of 5-6 from 150 to 250 °C.

379 In order to investigate the role of Dy^{3+} in controlling the solubility of Dy hydroxide in our
380 experiments, we conducted a series of test optimizations in which only the Dy^{3+} species was
381 considered in the speciation calculations. These optimization tests result in poor agreement (typical
382 residuals of 4 to 13%) with the experimental solubility data for REE phosphates at pH 2 (from
383 Gysi et al., 2015) and REE hydroxides (this study) in the higher pH range (Fig. S3). This
384 discrepancy is especially pronounced at 200 and 250 °C. Conversely, solubility calculated using
385 optimizations that include the Dy hydroxyl species in the equilibrium speciation and optimization
386 calculations are in much better agreement with our experimental solubility data and those for the
387 REE phosphates (Fig. 6; with residuals generally <3 % in Table S4). Thus, it is clear that the
388 inclusion of the Dy hydroxyl species in the optimizations is necessary.

389 Finally, comparison of the calculated pH values from this study with those measured by
390 Wood et al. (2002) based on the solubility of Nd hydroxide (Fig. 7) indicates that their
391 potentiometric data closely overlap with the optimized pH values calculated from our experimental
392 data. In contrast, pH values predicted using Supcrt92 results in an erroneously low pH range (~2.5-
393 3.5) for the solubility of Dy hydroxide. The pH values measured by Deberdt et al. (1998) between
394 40 to 90 °C for the solubility of La and Gd hydroxide indicate an overall consistency of the reported
395 pH ranges in aqueous solutions equilibrated with REE hydroxide solids. Hence, this comparison
396 gives confidence that the speciation obtained in this study from batch-type experiments and the
397 thermodynamic optimizations yield reasonable pH values in accordance with other experimental
398 approaches.

399

400 *4.4. Recommended equilibrium constants for predicting the Dy hydroxide solubility and the*
401 *hydrolysis of* Dy^{3+}

402 Revised equilibrium constants for the dissolution of Dy hydroxide (K_{s0}) and the formation of Dy
403 hydroxyl complexes (β_1-β_3, Eqs. 3-6) were calculated at each temperature from the relation:

404 $$\log K = -\Delta_r G°_T/\mathrm{RTln}(10) \quad (8)$$

405 using the optimized standard Gibbs energy values from the fits in Table 4, where R is the ideal gas
406 constant in $J \cdot mol^{-1}K^{-1}$ and T is the temperature in Kelvin. The equilibrium constants were fit as a
407 function of temperature expressed as the following equation:

408 $$\log K = A_0 + A_1 T + A_2/T + A_3 \ln T + A_4/T^2 \quad (9)$$

409 where T is in Kelvin and A_0-A_4 are the fitted regression coefficients listed in Table 5. This
410 expanded equation was derived using the smoothed fits generated from the standard Gibbs energies
411 from Table 4.

412 The logarithm of the solubility products ($\log K_{s0}$) derived for Dy hydroxide was calculated
413 using the optimized $\Delta_f G°_T$ from this study and the 25 °C $\Delta_f G°$ from Pan et al. (2024) for Dy^{3+}
414 (Table 3) in combination with the $\Delta_f G°_T$ values for Dy hydroxide from Diakonov et al. (1998) and
415 OH^- from Table S2. The $\log K_{s0}$ values decrease from -23.9 at 25 °C to -26.8 at 250 °C (Fig. 8)
416 indicating that the solubility of Dy hydroxide is retrograde. The decline in solubility is relatively
417 minor between 25 and 150 °C with $\log K_{s0}$ values decreasing by less than 0.5 log unit, whereas
418 between 150 and 250 °C the $\log K_{s0}$ values decrease by more than 2 orders of magnitude. The
419 solubility products calculated from the $\Delta_f G°$ values for the Dy^{3+} aqua ion at reference conditions
420 of 25 °C and 1 bar derived from Pan et al. (2024) combined with the HKF parameters from Haas
421 et al. (1995) are in excellent agreement with the regressed curve fitted to our data (Fig. 8).

422 To our knowledge, only three experimental studies measured the solubility products of Dy
423 hydroxide at ambient temperature including Aksel'rud and Spivakovskii (1960), Kovalenko et al.

(1966), and Orhanović et al. (1966) (Table S6). Aksel'rud and Spivakovskii (1960) conducted potentiometric experiments in which Dy hydroxide was precipitated from $DyCl_3$-NaCl solutions with pH values of 5.6 to 7.2 with an equilibration time of 50 days resulting in a reported $\log K_{s0}$ value at 25 °C of -25.9 ± 0.3. Kovalenko et al. (1966) conducted a titration study in which Dy hydroxide was precipitated from solutions with initial log molality $DyCl_3$ concentrations of -5.9 to -5.3 which resulted in the derivation of a $\log K_{s0}$ value at 20 °C of -25.0. Orhanović et al. (1966) conducted titration experiments in which Dy hydroxide was precipitated from $Dy(NO_3)_3$ solutions at 20 °C and allowed to equilibrate for 24 hours to determine a $\log K_{s0}$ value of -23.9. The latter study is in excellent agreement with our recommended $\log K_{s0}$ value derived at 25 °C based on the optimized Dy^{3+} aqua ion $\Delta_f G°$ value derived by Pan et al. (2024) in Table 3. In contrast, the Dy^{3+} aqua ion $\Delta_f G°$ value from Supcrt92 results in a calculated $\log K_{s0}$ values of -27.8 which is four orders of magnitude lower than derived by either extrapolation of our solubility product data to 25 °C, or using the data form Pan et al. (2024) or Orhanović et al. (1966). The $\log K_{s0}$ values derived by Aksel'rud and Spivakovskii (1960) and Kovalenko et al. (1966) are 1-2 orders of magnitude lower than our study, which could result from their thermodynamic evaluation of the retrieved experimental data which is difficult to trace from the information given in those studies. Finally, the $\log K_{s0}$ values compiled by Diakonov et al. (1998b) range between -24.5 to -28.0, noting however, that the thermodynamic properties used for the Dy^{3+} aqua ion in their study has a $\Delta_f G°$ value of -663.0 kJ/mol 25 °C, which is inconsistent with the optimized value of -686.8 kJ/mol from Table 3 and would fall too far off from the linear trend observed in a $\Delta_f G°$ vs. T diagram (Fig. 5).

The revised formation constants for Dy hydroxyl complexes (β_1-β_3) derived from our study (Table 5) exhibit an overall trend of slight decrease between 25 and 100 °C followed by an increase at higher temperatures (Fig. 9). The revised $\log\beta$ values derived in this study of 6.1 ($\log\beta_1$), 11.7 ($\log\beta_2$), and 16.9 ($\log\beta_3$) are consistent with the values calculated using Supcrt92 at 25 °C.

448 However, from 100 to 250 °C the logβ values from this study are 1.5 to 3.0 log units lower than
449 those of Suprcrt92 (Table S7, Fig. 9), indicating that Supcrt92 significantly over estimates the
450 formation of Dy hydroxyl species over this temperature range. Literature values for log$\beta_{1\text{-}3}$ for
451 Dy^{3+} come from experimental (Luo et al., 1990; Klungness and Byrne, 2000) and correlation
452 studies (Baes and Mesmer, 1976; Lee and Byrne, 1992). The study by Baes and Mesmer (1976)
453 used correlations between experimental data available at that time for REE hydroxyl species to
454 estimate formation constants for the first through fourth hydrolysis of Dy^{3+}, reporting estimated
455 values of 6.0 for logβ_1, 11.8 for logβ_2, and 17.3 for logβ_3 at 25 °C. Similarly, Lee and Byrne (1992)
456 assessed the available experimental data for REE hydroxyl species to determine linear free energy
457 relationships that they used to estimate equilibrium constants for REE hydroxyl complexes
458 yielding estimated logβ_1 of 6.19, logβ_2 of 11.9, and logβ_3 of 17.16 at 25 °C. Luo et al. (1990)
459 conducted an equilibrium-pH study to determine the first hydrolysis constant for Dy^{3+} in 2 molar
460 nitric acid solutions, using various means to estimate a conditional logβ_1 of ~5.45 for Dy^{3+} in a
461 solution having 0 ionic strength. However they cautioned that the formation of Dy nitrate
462 complexes was not taken into account when estimating the conditional logβ_1. Klungness and Byrne
463 (2000) used both potentiometric and spectrophotometric experiments to measure logβ_1 in Dy
464 bearing solutions having 0.7 molar ionic strength at temperatures of 25, 40, and 55 °C to determine
465 the temperature dependence of logβ_1, and used an experimentally determined ionic strength
466 dependence for hydrolysis of Ho^{3+} to estimate the ionic strength dependence of logβ_1 for Dy^{3+}.
467 Based on these experiments, Klungness and Byrne (2000) report an experimental logβ_1 of 6.11 for
468 an 0.7 ionic strength solution and estimate a logβ_1 of 6.41 for 0 ionic strength solutions at 25 °C,
469 a value 0.65 log units lower than the logβ_1 derived in this study. With the exception of the
470 conditional logβ_1 of Luo et al. (1990), which is problematic as discussed above, the literature values
471 for logβ_1 are in good agreement (±0.3 log unit) with the revised logβ_1 calculated at 25 °C using the

temperature function in this study (Table 5). The values for logβ_2 and logβ_3 from Baes and Mesmer, (1976) and Lee and Byrne (1992) are also in excellent agreement with the revised logβ_2 and logβ_3 reported in this study in Table 5.

5. CONCLUSIONS

The solubility data generated in this study allow derivation of the solubility products of Dy hydroxide and the formation constants (β_1 to β_3) of Dy hydroxyl complexes between 25 and 250 °C. Importantly, the optimized thermodynamic properties are internally consistent with experimental solubility data for $DyPO_4$ xenotime collected between 100 and 250 °C (Gysi et al., 2015). There is now a strong evidence that the REE^{3+} aqua ion properties tabulated by Shock and Helgeson (1988) and Shock et al. (1997), and the REE hydroxyl complexes tabulated by Haas et al. (1995) need to be revised. This is in line with the experimental study of the properties of Nd^{3+} by Wood et al. (2002) and as suggested in the comprehensive optimization study by Pan et al. (2024) for all of the REE^{3+} aqua ions based on solubility data for the monazite and xenotime endmembers. Our solubility data indicate that the Dy^{3+} aqua ion is more stable relative to Dy hydroxyl complexes in the studied pH and temperature range in comparison to the predicted speciation based on the thermodynamic data for aqueous species from Haas et al. (1995) or Supcrt92. The large corrections necessary for the Dy^{3+} aqua ion (-21 to -26 kJ/mol in $\Delta_f G°_T$ values) have important implications for the derivation of the thermodynamic properties of other REE aqueous species and for the prediction of REE mineral solubilities in hydrothermal acidic fluids.

ACKNOWLEDGMENTS

This research is based upon work supported by the U.S. Department of Energy, Office of Science, Office of Basic Energy Sciences, Geosciences program under Award Numbers DE-SC0021106

and DE-SC0022269. Raman analyses at the New Mexico Bureau of Geology and Mineral Resources were supported through a EAR-2117061 major research instrumentation grant from the National Science Foundation. We would like to thank Hannah Juan Han and Bonnie Frey at the New Mexico Bureau of Geology for their assistance on the ICP-OES and ICP-MS instruments. We are grateful to two anonymous reviewers for their constructive comments. We also thank Editor-in-Chief O. Pokrovsky for the editorial handling.

DATA AVAILABILITY

Data are available through Mendeley Data at https://doi.org/10.17632/dppg58d6s2.1

ELECTRONIC APPENDIX. Supplementary Material

The Supplementary data file contains Raman analysis (Table S1), thermodynamic background data (Table S2), calculated speciation using Supcrt92 (Table S3, Fig. S1), optimized speciation calculations using GEMSFITS (Table S4), composite scaled sensitivity of each fitted Dy species, and the correlations between fitted species (Table S5), compilation of solubility constants for Dy hydroxide (Table S6), comparison of equilibrium constants calculated in this study and using thermodynamic parameters from Supcrt92 (Table S7), Dy speciation and solubility as activity vs. optimized pH showing the changes in slope with pH (Fig. S2), and test optimization calculations assuming only Dy^{3+} controls speciation (Fig. S3).

REFERENCES

Aksel'rud, N.V., Spivakovskii, V.B., 1960. Basic chlorides and hydroxides of dysprosium. Zhur. Neorg. Khim., 5.

Baes, C.F., Mesmer, R.E., 1976. The Hydrolysis of Cations 1976. Malabar, Fla.: RE Krieger.

Baes Jr, C.F. Mesmer, R.E., 1981. Thermodynamics of cation hydrolysis. Am. J. Sci, 281, 935-962.

Beall G. W., Milligan W. O. and Wolcott H. A. 1977. Structural trends in the lanthanide trihydroxides. J. Inorg. Nucl. Chem. 39, 65–70.

Cui, J., Hope, G.A. 2015. Raman and Fluorescence Spectroscopy of CeO_2, Er_2O_3, Nd_2O_3, Tm_2O_3, Yb_2O3, La_2O_3, and Tb_4O_7. J. Spectrosc. 2015.

Choppin, G. R., Kelly, D. A., Ward, E. H., 1966. The effect of changes in the ionic medium on the stability constant of $Eu(NO_3)^{2+}$. AEC Access. Nos. ORO–1797–2.

Deberdt, S., Castet, S., Dandurand, J.-L., Harrichoury, J.-C., Louiset, I., 1998. Experimental study of $La(OH)_3$ and $Gd(OH)_3$ solubilities (25 to 150°C), and La–acetate complexing (25 to 80°C). Chem. Geol. 151, 349–372.

Diakonov, I. I., Tagirov, B. R., Ragnarsdottir, K. V., 1998a, Standard Thermodynamic Properties and Heat Capacity Equations for Rare Earth Element Hydroxides: Radiochim. Acta, 81, 107–116.

Diakonov, I.I., Ragnarsdottir, K.V, Tagirov, B.R., 1998b. Standard thermodynamic properties and heat capacity equations of rare earth hydroxides: II. Ce(III)-, Pr-, Sm-, Eu(III)-, Gd-, Tb-, Dy-, Ho-, Er-, Tm-, Yb-, and Y-hydroxides. Comparison of thermochemical and solubility data. Chem. Geol. 151, 327–347.

Guan, Q., Mei, Y., Etschmann, B., Louvel, M., Testemale, D., Bastrakov, E., Brugger, J., 2022a. Yttrium speciation in sulfate-rich hydrothermal ore-forming fluids. Geochim. Cosmochim. Acta, 325, 278–295.

Guan, Q., Mei, Y., Etschmann, B., Louvel, M., Testemale, D., Spezia, R., Brugger, J., 2022b. Speciation and thermodynamic properties of La (III)-Cl complexes in hydrothermal fluids: A

543 combined molecular dynamics and in situ X-ray absorption spectroscopy study. Geochim.
544 Cosmochim. Acta, 330, 27–46.
545 Gysi, A.P., Harlov, D., 2021. Hydrothermal solubility of $TbPO_4$, $HoPO_4$, $TmPO_4$, and $LuPO_4$
546 xenotime endmembers at pH of 2 and temperatures between 100 and 250 C. Chem. Geol. 567,
547 120072.
548 Gysi, A.P., Williams-Jones, A.E., Harlov, D., 2015. The solubility of xenotime-(Y) and other
549 HREE phosphates ($DyPO_4$, $ErPO_4$ and $YbPO_4$) in aqueous solutions from 100 to 250 °C and
550 P_{sat}. Chem. Geol. 401, 83–95.
551 Gysi, A.P., Williams-Jones, A.E., Collins, P., 2016. Lithogeochemical Vectors for Hydrothermal
552 Processes in the Strange Lake Peralkaline Granitic REE-Zr-Nb Deposit. Econ. Geol. 111,
553 1241–1276.
554 Gysi A.P., Harlov D., Miron G.D., 2018. The solubility of monazite ($CePO_4$), $SmPO_4$, and $GdPO_4$
555 in aqueous solutions from 100 to 250 °C. Geochim. Cosmochim. Acta 242, 143–164.
556 Gysi, A.P., Hurtig, N.C., Pan, R., Miron, G.D., and Kulik, D.A., 2023. MINES thermodynamic
557 database, New Mexico Bureau of Geology and Mineral Resources, version 23,
558 https://doi.org/10.58799/mines-tdb.
559 Han, H.J., Gysi, A.P., 2024. UV-Vis spectrophotometric determination of rare earth elements
560 (REE) speciation at near-neutral to alkaline pH. Part I: m-cresol purple properties from 25–75°
561 C and Er hydrolysis. Dalton Trans., 53, 13129-13141.
562 Haas, J.R., Shock, E.L., Sassani, D.C., 1995. Rare earth elements in hydrothermal systems:
563 Estimates of standard partial molal thermodynamic properties of aqueous complexes of the
564 rare earth elements at high pressures and temperatures. Geochim. Cosmochim. Acta, 59, 4329–
565 4350.

566 Helgeson, H.C., Kirkham, D.H., Flowers, G.C., 1981. Theoretical prediction of the
567 thermodynamic behavior of aqueous electrolytes by high pressures and temperatures; IV,
568 Calculation of activity coefficients, osmotic coefficients, and apparent molal and standard and
569 relative partial molal properties to 600 °C and 5kb. Am. J. Sci. 281, 1249–1516.
570 Hurtig, N.C., Gysi, A.P., Smith-Schmitz, S.E., Harlov, D., 2024. Raman spectroscopic study of
571 anhydrous and hydrous REE phosphates, oxides, and hydroxides. Dalton Trans. 53, 9964-
572 9978.
573 Johnson, J.W., Oelkers, E.H., Helgeson, H.C., 1992. SUPCRT92: A software package for
574 calculating the standard molal thermodynamic properties of minerals, gases, aqueous species,
575 and reactions from 1 to 5000 bar and 0 to 1000°C. Comput. Geosci. 18, 899–947.
576 Kielland, J. 1937. Individual activity coefficients of ions in aqueous solutions. J. Am. Chem. Soc.
577 59, 1675-1678.
578 Kestin J., Sengers J.V., Kamgar-Parsi B., Levelt Sengers J. M.H., 1984. Thermophysical properties
579 of fluid H_2O. J. Phys. Chem. Ref. Data 13, 175–183.
580 Klungness, G.D., Byrne, R.H., 2000. Comparative hydrolysis behavior of the rare earths and
581 yttrium: the influence of temperature and ionic strength. Polyhedron, 19, 99-107.
582 Konings, R.J., Beneš, O., Kovács, A., Manara, D., Sedmidubský, D., Gorokhov, L., Iorish, V.S.,
583 Yungman, V., Shenyavskaya, E., Osina, E. 2014. The thermodynamic properties of the f-
584 elements and their compounds. Part 2. The lanthanide and actinide oxides. J. Phys. Chem. Ref.
585 Data, 43, 1.
586 Kovalenko, P.N., Azhipa, L.T., Evstifeev, M.M., 1966. Oscillographic determination of the pH of
587 precipitation and activity products of ytterbium and neodimium hydroxides. Russ. Jour. Inorg.
588 Chem. 11, 1443-1445.

589 Kulik, D.A., Wagner, T., Dmytrieva, S.V., Kosakowski, G., Hingerl, F.F., Chudnenko, K.V.,
590 Berner, U.R., 2013. GEM-Selektor geochemical modeling package: revised algorithm and
591 GEMS3K numerical kernel for coupled simulation codes. Comput. Geosci. 17. 1–24
592 Lee, J.H. and Byrne, R.H., 1992. Examination of comparative rare earth element complexation
593 behavior using linear free-energy relationships. Geochim. Cosmochim. Acta, 56, 1127-1137.
594 Loges, A., Migdisov, A.A., Wagner, T., Williams-Jones, A.E., Markl, G., 2013. An experimental
595 study of the aqueous solubility and speciation of Y(III) fluoride at temperatures up to 250°C.
596 Geochim. Cosmochim. Acta, 123, 403–415.
597 Louvel, M., Bordage, A., Testemale, D., Zhou, L., Mavrogenes, J., 2015. Hydrothermal controls
598 on the genesis of REE deposits: Insights from an in situ XAS study of Yb solubility and
599 speciation in high temperature fluids (T< 400° C). Chem. Geol. 417, 228–237.
600 Louvel, M., Etschmann, B., Guan, Q., Testemale, D., Brugger, J., 2022. Carbonate complexation
601 enhances hydrothermal transport of rare earth elements in alkaline fluids. Nature Comm. 13,
602 1456.
603 Luo, Q., Shen, M., Ding, Y., Bao, X., Dai, A., 1990. Studies on hydrolytic polymerization of rare-
604 earth metal ions—V Hydrolytic polymerization of Dy^{3+}. Talanta, 37, 357-360.
605 Lutterotti L., Matthies S., Wenk H-R., 1999. MAUD (Material Analysis Using Diffraction): a user
606 friendly Java program for Rietveld texture analysis and more. Proceeding of the Twelfth
607 International Conference on Textures of Materials (ICOTOM-12), 1, 1599-1604.
608 Migdisov, A.A., Williams-Jones, A.E. 2002. A spectrophotometric study of neodymium (III)
609 complexation in chloride solutions. Geochim. Cosmochim. Acta, 66, 4311–4323.
610 Migdisov, A.A., Williams-Jones, A.E. 2007. An experimental study of the solubility and
611 speciation of neodymium (III) fluoride in F-bearing aqueous solutions. Geochim. Cosmochim.
612 Acta, 71, 3056-3069.

Migdisov, A.A., Williams-Jones, A.E. 2014. Hydrothermal transport and deposition of the rare earth elements by fluorine-bearing aqueous liquids. Mineral. Deposita, 49, 987–997.

Migdisov, A.A., Williams-Jones, A.E., Brugger, J., Caporuscio, F.A., 2016. Hydrothermal transport, deposition, and fractionation of the REE: Experimental data and thermodynamic calculations. Chem. Geol. 439, 13–42.

Miron, G.D., Kulik, D.A., Dmytrieva, S.V., Wagner, T., 2015. GEMSFITS: Code package for optimization of geochemical model parameters and inverse modeling. Appl. Geochem. 55, 28–45.

Morss, L.R., Konings, R.J.M., 2004. Thermochemistry of binary rare earth oxides. In: Adachi, G., Imanaka, N., Kang, Z.C. (Eds.), Binary Rare Earth Oxides. Kluwer Academic Publishers, Dordrecht. 163–188.

Orhanović, Z., Pokrić, B., Furedi, H. and Branica, M., 1966. Precipitation and hydrolysis of metallic ions. III. Studies on the solubility of yttrium and some rare earth hydroxides. Croat. Chem. Acta, 38, 269-276.

Pan, R., Gysi, A.P., Miron, G.D., Zhu, C., 2024. Optimized thermodynamic properties of REE aqueous species (REE^{3+} and $REEOH^{2+}$) and experimental database for modeling the solubility of REE phosphate minerals (monazite, xenotime, and rhabdophane) from 25 to 300 °C. Chem. Geol. 643, 121817.

Patel, A. K., Upadhyay, D., Mishra, B., Pruseth, K. L., 2023. Reconstruction of hydrothermal fluid composition of the Kamthai carbonatite complex, India using lattice strain model: Implications for LREE/HREE fractionation. Lithos, 444, 107097.

Perry, E.P., Gysi, A.P., 2018. Rare earth elements in mineral deposits: speciation in hydrothermal fluids and partitioning in calcite. Geofluids, 2018, 5382480.

Nisbet, H., Migdisov, A. A., Goncharov, V., van Hinsberg, V., Williams-Jones, A. E., Xu, H., Guo, X., 2022. The solubility and speciation of Nd in carbonate-bearing hydrothermal fluids up to 250 °C. Chem. Geol. 611, 121122.

Robinson, R., Stokes, R., 1968. Electrolyte solutions (2nd Edn). London.

Sanivarapu, S.R., Lawrence, J.B., Sreedhar, G. 2018. Role of surface oxygen vacancies and lanthanide contraction phenomenon of $Ln(OH)_3$ (Ln= La, Pr, and Nd) in sulfide-mediated photoelectrochemical water splitting. ACS omega, 3, 6267-6278.

Shock, E.L., Helgeson, H.C., 1988. Calculation of the thermodynamic and transport properties of aqueous species at high pressures and temperatures: Correlation algorithms for ionic species and equation of state predictions to 5 kb and 1000°C. Geochim. Cosmochim. Acta, 52, 2009–2036.

Shock, E.L., Oelkers, E.H., Johnson, J.W., Sverjensky, D.A., Helgeson, H.C., 1992. Calculation of the thermodynamic properties of aqueous species at high pressures and temperatures. Effective electrostatic radii, dissociation constants and standard partial molal properties to 1000 °C and 5 kbar. J. Chem. Soc. Faraday T. 88, 803–826.

Shock, E.L., Sassani, D.C., Willis, M., Sverjensky, D.A., 1997. Inorganic species in geologic fluids: Correlations among standard molal thermodynamic properties of aqueous ions and hydroxide complexes. Geochim. Cosmochim. Acta, 61, 907–950.

Tanger, J.C., Helgeson, H.C., 1988. Calculation of the thermodynamic and transport properties of aqueous species at high pressures and temperatures; revised equations of state for the standard partial molal properties of ions and electrolytes. Am. J. Sci. 288, 19–98.

Wagner, T., Kulik, D.A., Hingerl, F.F., Dmytrieva, S.V., 2012. GEM-Selektor geochemical modeling package: TSolMod C++ class library and data interface for multicomponent phase models. Can. Mineral. 50, 1173–1195.

660 Wan, Y., Wang, X., Chou, I. M., Li, X., 2021. Role of sulfate in the transport and enrichment of
661 REE in hydrothermal systems. Earth Planet. Sci. Lett. 569, 117068.
662 Watari, T., Nansai, K., Nakajima, K., 2020. Review of critical metal dynamics to 2050 for 48
663 elements. Resour. Conserv. Recycl. 155, 104669.
664 Wojdyr, M., 2010. Fityk: a general-purpose peak fitting program. J. Appl. Crystallogr. 43, 1126-
665 1128.
666 Wood, S.A., Palmer, D.A., Wesolowski, D.J., Bénézeth, P., 2002. The aqueous geochemistry of
667 the rare earth elements and yttrium. Part XI. The solubility of $Nd(OH)_3$ and hydrolysis of Nd^{3+}
668 from 30 to 290 °C at saturated water vapor pressure with *in-situ* pH_m measurement. In:
669 Hellmann, R., Wood, S.A. (Eds.), Water–rock interactions, ore deposits, and environmental
670 geochemistry: a tribute to David Crerar, Special Publication, 7, 229–256.
671 Zeng, Q.G., Ding, Z.J., Zhang, Z.M., Sheng, Y.Q. 2010. Photoluminescence and Raman
672 spectroscopy studies of $Eu(OH)_3$ rods at high pressures. J. Phys. Chem. C, 114, 4895-4900.
673

674 TABLES

675 **Table 1.** Crystal lattice parameters of $Dy(OH)_3(s)$ in the hexagonal P63/m crystal structure
676 derived from Rietveld refinement of powder XRD data.

Source of data	*a* (Å)	*c* (Å)	*α* (°)	*γ* (°)
This study	6.287	3.575	90.1	119.9
Beall et al. (1977)	6.286	3.577	90.0	120.0

677

Table 2. Starting pH, reaction times, and Dy compositions (logarithm molality, mol/kg) of the quenched experimental solutions after equilibration with Dy hydroxide solids at temperatures of 150, 200, and 250 °C at saturated water vapor pressure. Dysprosium concentrations were measured using ICP-OES unless otherwise noted.

Time (days)	T (°C)	$pH_{init,25°C}$[a]	log ($m$$ClO_4^-$) (mol/kg)	log (mDy) (mol/kg)	Type[b]
15	150	2.0	-1.96	-2.46	Eq
18	150	2.0	-1.96	-2.44	Eq
21	150	2.0	-1.96	-2.46	Eq
15	150	2.5	-2.48	-3.01	Eq
18	150	2.5	-2.48	-3.04	Eq
21	150	2.5	-2.48	-2.98	Eq
1	150	3.0	-2.99	-5.15	K
3	150	3.0	-2.99	-4.32	K
6	150	3.0	-2.99	-3.80	K
9	150	3.0	-2.99	-3.60	K
9	150	3.0	-2.99	-3.64	K
12	150	3.0	-2.99	-3.77	K
12	150	3.0	-2.99	-3.63	K
15	150	3.0	-2.99	-3.61	Eq
18	150	3.0	-2.99	-3.53	Eq
21	150	3.0	-2.99	-3.60	Eq
24	150	3.0	-2.99	-3.59	Eq
15	150	3.5	-3.49	-4.11	Eq
18	150	3.5	-3.49	-4.08	Eq
21	150	3.5	-3.49	-3.98	Eq
15	150	4.0	-4.00	-4.53	Eq
18	150	4.0	-4.00	-4.49	Eq
21	150	4.0	-4.00	-4.48	Eq
15	150	4.5	-4.50	-4.96	Eq
18	150	4.5	-4.50	-4.82	Eq
21	150	4.5	-4.50	-4.88	Eq
15	150	5.0	-5.00	-5.34	Eq
18	150	5.0	-5.00	-5.30	Eq
21	150	5.0	-5.00	-5.34	Eq
15	200	2.0	-1.96	-2.44	Eq
18	200	2.0	-1.96	-2.43	Eq

682 **Table 2.** (Continued)

Time (days)	*T* (°C)	$pH_{init,25°C}$[a]	log (*m*ClO_4^-) (mol/kg)	log (*m*Dy) (mol/kg)	Type[b]
15	200	2.5	-2.48	-2.95	Eq
18	200	2.5	-2.48	-2.94	Eq
15	200	3.0	-2.99	-3.55	Eq
18	200	3.0	-2.99	-3.57	Eq
15	200	3.5	-3.49	-3.97	Eq
18	200	3.5	-3.49	-4.01	Eq
15	200	4.0	-4.00	-4.51	Eq
18	200	4.0	-4.00	-4.55	Eq
15	200	4.5	-4.50	-5.04	Eq
18	200	4.5	-4.50	-4.94	Eq
15	200	5.0	-5.00	-5.67	Eq
18	200	5.0	-5.00	-5.62	Eq
1	250	2.0	-1.96	-3.69	K
3	250	2.0	-1.96	-3.22	K
6	250	2.0	-1.96	-2.93	K
8	250	2.0	-1.96	-2.90	K
10	250	2.0	-1.96	-2.72	Eq
12	250	2.0	-1.96	-2.69	Eq
14	250	2.0	-1.96	-2.71	Eq
18	250	2.0	-1.96	-2.55	Eq
21	250	2.0	-1.96	-2.57	Eq
10	250	2.5	-2.48	-3.16	Eq
12	250	2.5	-2.48	-3.08	Eq
14	250	2.5	-2.48	-3.09	Eq
18	250	2.5	-2.48	-3.04	Eq
10	250	3.0	-2.99	-3.70	Eq
12	250	3.0	-2.99	-3.53	Eq
14	250	3.0	-2.99	-3.55	Eq
18	250	3.0	-2.99	-3.53	Eq
10	250	3.5	-3.49	-4.34	Eq
12	250	3.5	-3.49	-4.29	Eq
14	250	3.5	-3.49	-4.16	Eq
18	250	3.5	-3.49	-4.28	Eq

683

Table 2. (Continued)

Time (days)	*T* (°C)	$pH_{init,25°C}$[a]	log (*m*ClO_4^-) (mol/kg)	log (*m*Dy) (mol/kg)	Type[b]
21	250	3.5	-3.49	-4.16	Eq
11	250	4.0	-4.00	-5.09	Eq
13	250	4.0	-4.00	-5.01	Eq
16	250	4.0	-4.00	-4.92	Eq
11	250	4.0	-4.00	-5.09	Eq
13	250	4.0	-4.00	-5.01	Eq
16	250	4.0	-4.00	-4.92	Eq
18	250	4.0	-4.00	-4.88	Eq
21	250	4.0	-4.00	-4.98	Eq
13	250	4.5	-4.50	-5.99	Eq
16	250	4.5	-4.50	-5.86	Eq
18	250	4.5	-4.50	-5.92	Eq
22	250	4.5	-4.50	-5.89	Eq
11	250	5.0	-5.00	-6.86[c]	Eq
13	250	5.0	-5.00	-6.85[c]	Eq
18	250	5.0	-5.00	-6.82[c]	Eq
21	250	5.0	-5.00	-6.92[c]	Eq

[a] Starting pH of the perchloric acid-based experimental buffer solutions at

[a] Starting pH of the perchloric acid-based experimental buffer solutions at 25 °C and 1 bar before reaction with Dy hydroxide.

[b] K = Kinetic experiments not used in optimization calculations; Eq = Equilibrium experiments used for optimization calculations.

[c] Dy concentration measured using ICP-MS.

Table 3. Optimized standard partial molal Gibbs energy of formation at temperature T and saturated water vapor pressure ($\Delta_f G°_T$) for Dy aqueous species based on thermodynamic parameter optimizations using GEMSFITS and the solubility data from Table 2. For comparison the initial values from Supcrt92 before optimization and values from Pan et al. (2004) are also listed. Fit statistics are listed in Table S5.

T (°C)	Ref[a]		$\Delta_f G°_T$ (Dy^{3+}) (J/mol)	$\Delta_f G°_T$ ($DyOH^{2+}$) (J/mol)	$\Delta_f G°_T$ ($Dy(OH)_2^+$) (J/mol)	$\Delta_f G°_T$ ($Dy(OH)_3^0$) (J/mol)
25	(Supcrt92)		-663,997	-856,465	-1,046,370	-1,233,814
25	(Pan et al.)		-686,850	-879,318	-1,069,223	-1,256,667
		Δ[b]	-22,853	-22,853	-22,853	-22,853
100	(Supcrt92)		-645,710	-852,329	-1,051,760	-1,248,610
100	(Pan et al.)		-668,563	-875,182	-1,074,614	-1,271,462
100	(this study)		-666,835	-857,281	-1,056,713	-1,253,562
		Δ[b]	-21,125	-4,952	-4,953	-4,952
		Opt[c,d]	O	O	R[e]	R[e]
150	(Supcrt92)		-632,513	-848,903	-1,054,383	-1,256,366
150	(Pan et al.)		-655,366	-871,755	-1,077,236	-1,279,218
150	(this study)		-658,802	-857,121	-1,062,601	-1,264,584
		Δ[b]	-26,289	-8,218	-8,218	-8,218
		Opt[d]	O	O	R[e]	R[e]
200	(Supcrt92)		-618,337	-844,876	-1,056,392	-1,262,894
200	(Pan et al.)		-641,190	-867,729	-1,079,246	-1,285,746
200	(this study)		-641,181	-852,493	-1,061,943	-1,268,444
		Δ[b]	-22,844	-7,617	-5,551	-5,550
		Opt[d]	O	O	O	R[f]
250	(Supcrt92)		-602,861	-840,063	-1,057,773	-1,268,373
250	(Pan et al.)		-625,714	-862,915	-1,080,627	-1,291,266
250	(this study)		-625,056	-845,952	-1,046,501	-1,257,101
		Δ	-22,195	-5,889	11,272	11,272
		Opt[d]	O	O	O	R[f]

[a] Ref: Supcrt92 (Shock and Helgeson, 1988; Haas et t al., 1995; Shock et al., 1997), Pan et al. (2024).
[b] Differences between Supcrt92 values and the optimized values used in this study.
[c] Optimizations based on the $DyPO_4$ monazite solubility data at pH 2 by Gysi et al. (2015) at 100 °C and based on the study by Pan et al. (2024) at 25 °C.
[d] Optimization type: O, optimized; R, reaction constrained. Reactions based on the thermodynamic data from Haas et al. (1995) according to: [e] $DyOH^{2+} + (n\text{-}1)H^+ = Dy(OH)_n^{3-n} + (n\text{-}1)H_2O$ at 100 and 150 °C; [f] $Dy(OH)_2^+ + H_2O = DyO_2H^0 + H^+$ at 200 and 250 °C.

705 **Table 4.** Regressed coefficients and R^2 values for fits of the temperature dependence of the
706 standard partial molal Gibbs energy of formation ($\Delta_f G°_T$ in J/mol) for aqueous Dy species
707 optimized in this study (Table 3). The fits are described by $\Delta_f G°_T = a + bT + c/T$, with T in
708 Kelvin.

Species	a×10^{-3}	*b*	c×10^{-4}	R^2	*T* range fit (°C)
Dy^{3+}	-861.1	384.4	1793.9	0.99	25-250
$DyOH^{2+}$	-728.0	-96.6	-3624.7	0.95	25-250
$Dy(OH)_2^{+}$	-1132.0	125.5	808.9	0.59	25-250
$Dy(OH)_3^{0}$	-1335.0	78.9	1687.4	0.23	25-250

709

Table 5. Regressed coefficients for the function expressing the logarithm of the solubility product ($\log K_{s0}$) for Dy hydroxide and the formation constants ($\log\beta_1$-β_3) for Dy hydroxyl species as a function of temperature from 25 to 250 °C. Regressions are generated using the optimized thermodynamic properties derived from Table 3, OH^- from Supcrt92 and Dy hydroxide from Diakonov et al. (1998b) (Table S2). The logarithm of the equilibrium constants ($\log K$) are expressed as a function of temperature: $\log K = A_0 + A_1T + A_2/T + A_3\ln T + A_4/T^2$, with T in Kelvin.

Reactions		logK (25 °C, 1 bar)	A_0	A_1	$A_2\times10^{-3}$	A_3	$A_4\times10^{-4}$
$Dy(OH)_3(s) = Dy^{3+} + 3OH^-$	(K_{s0})	-23.9	-2761.7	-0.407	162.8	427.6	-1095.9
$Dy^{3+} + OH^- = DyOH^{2+}$	(β_1)	6.1	962.0	0.137	-69.5	-146.3	622.3
$Dy^{3+} + 2OH^- = Dy(OH)_2^+$	(β_2)	11.7	1887.2	0.274	-110.9	-292.6	729.9
$Dy^{3+} + 3OH^- = Dy(OH)_3^0$	(β_3)	16.9	2826.5	0.411	-162.8	-438.9	1023.3

FIGURES:

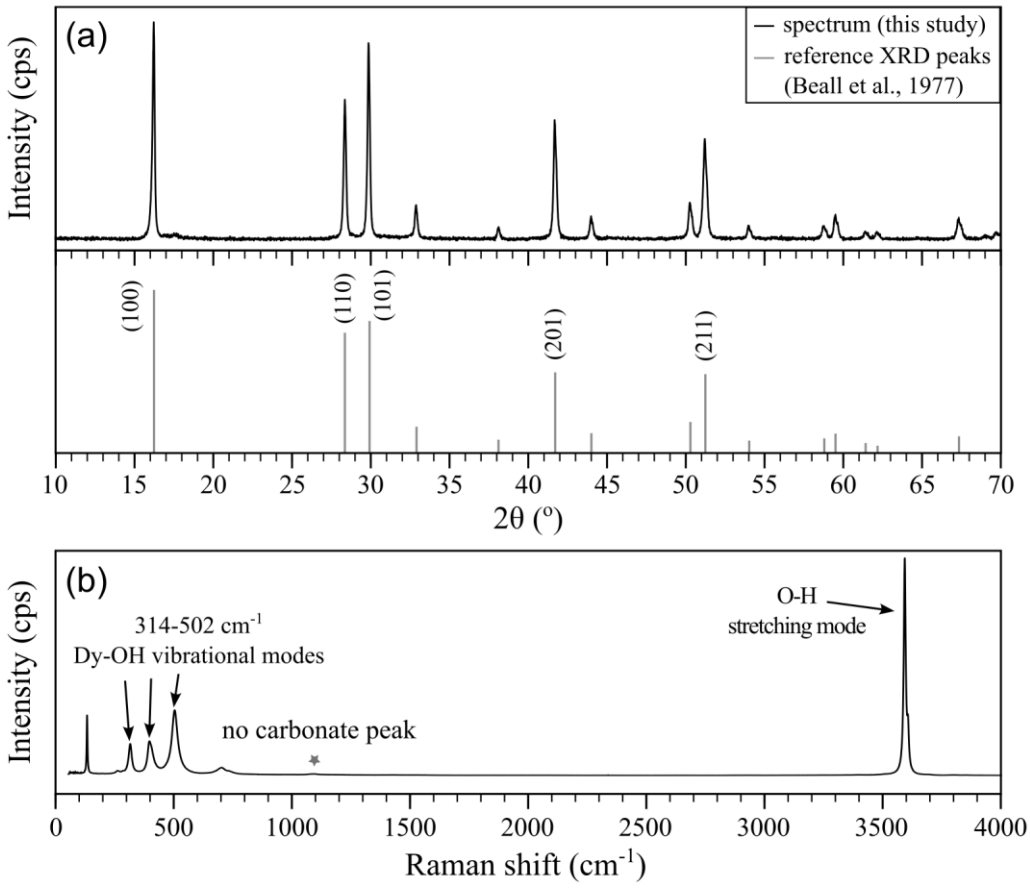

Figure 1. Powder XRD and Raman spectra of Dy hydroxide synthesized hydrothermally at 250 °C. (a) Comparison to the reference peak positions from XRD spectrum by Beall et al. (1977) for $Dy(OH)_3$(*s*) with the hexagonal P63/m crystal structure. The Miller indices for major reflections are indicated in brackets. (b) Raman spectrum showing the vibrational mode for Dy-OH and O-H stretching modes, with a lack of a carbonate mode at ~1090 cm^{-1} (gray star), indicating the synthesis of pure Dy hydroxide.

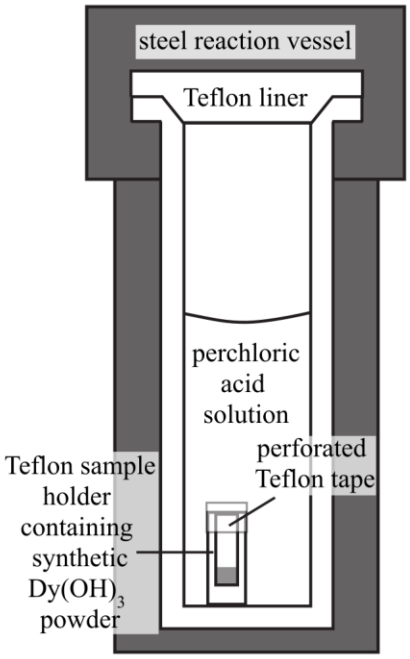

727

728 **Figure 2.** Schematic sketch of a fully assembled Teflon-lined batch-type Parr reaction vessel
729 showing the sample holder for Dy hydroxide powders with Teflon membrane, and perchloric acid
730 based experimental solutions.

731

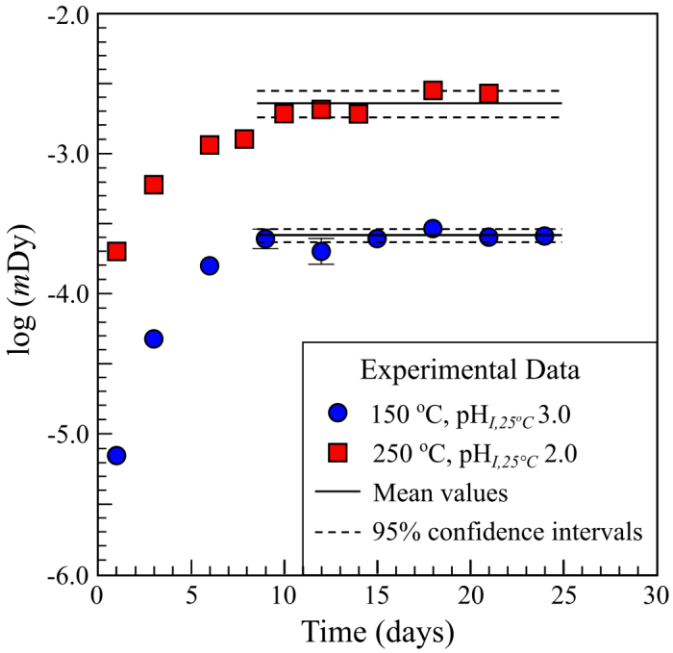

732

733 **Figure 3.** Kinetic experiments showing the logarithm of total dissolved Dy hydroxide molality (in
734 mol/kg) as a function of time (days) for experiments conducted at 150 and 250 °C and starting pH
735 at room temperature ($pH_{init.,25°C}$) of 3.0 and 2.0, respectively. Solid lines represent mean
736 concentrations calculated for experiments conducted for >9−10 days and indicate approach to
737 equilibrium between the perchloric acid based solutions and the Dy hydroxide powder. The 95%
738 confidence bounds are shown as dashed lines. Experimental data are listed in Table 2.

739

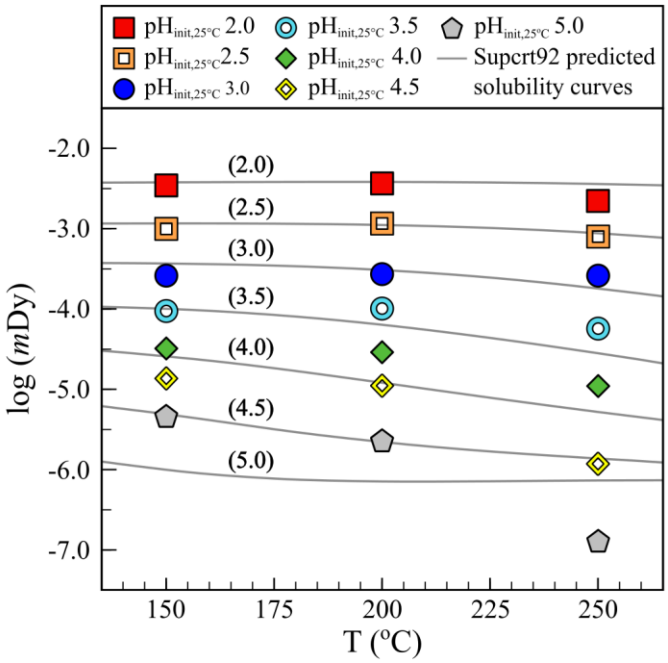

740

741 **Figure 4.** Logarithm of total dissolved Dy concentrations (mol/kg) measured in the quenched
742 experimental solutions as a function of temperature and starting pH at 25 °C (pH$_{init.,25°C}$) of the
743 perchloric acid based experimental starting solutions. Experimental uncertainties (1σ) are smaller
744 than the symbol sizes. Gray lines indicate the calculated Dy hydroxide solubility curves as a
745 function of temperature using the thermodynamic properties for aqueous Dy species from Supcrt92
746 and the mineral properties from Diakonov et al. (1998b) (Table S2). Values in brackets above each
747 line indicate the corresponding pH$_{init.,25°C}$ values for each model.

748

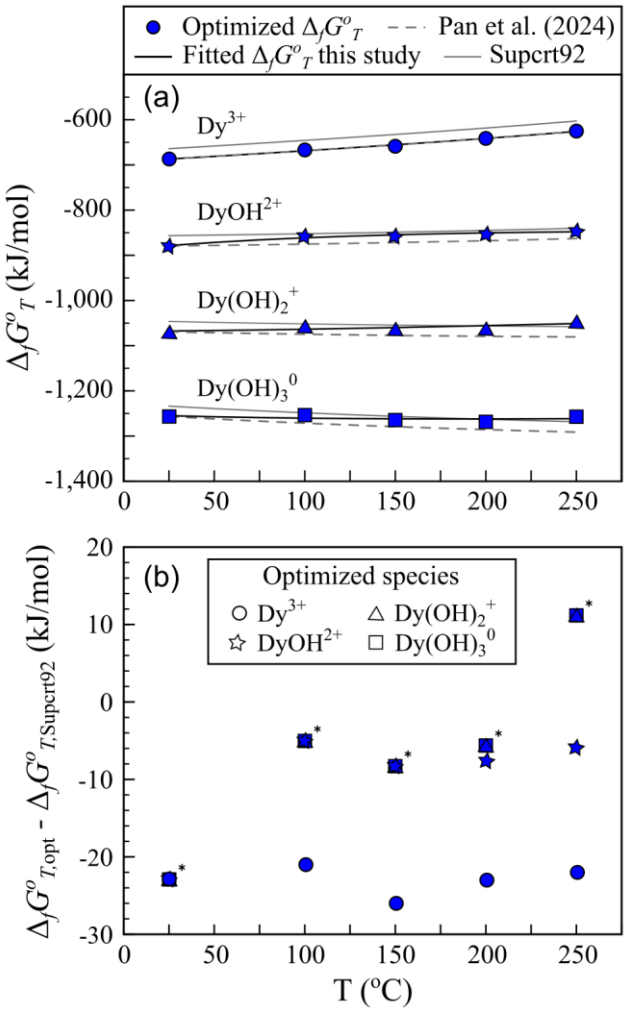

Figure 5. (a) Standard Gibbs energies of formation of aqueous Dy species (in kJ/mol) derived from the optimizations ($\Delta_f G^o_{T,\,opt}$) as a function of temperature (°C) and comparison to calculated $\Delta_f G^o_T$ values using the thermodynamic properties for aqueous species from Supcrt92 (Table S2) and from the study of Pan et al. (2024). The optimized $\Delta_f G^o_{T,\,opt}$ values are listed in Table 3 and the regressed fits as a function of temperature are listed in Table 4. (b) Difference between $\Delta_f G^o_{T,\,opt}$ and Supcrt92 ($\Delta_f G^o_{T,\,opt}$ - $\Delta_f G^o_{T,\,Supcrt}$) as a function of temperature. Symbols marked with an asterisk (*) indicate overlapping species fixed by reaction constraints (Table 3).

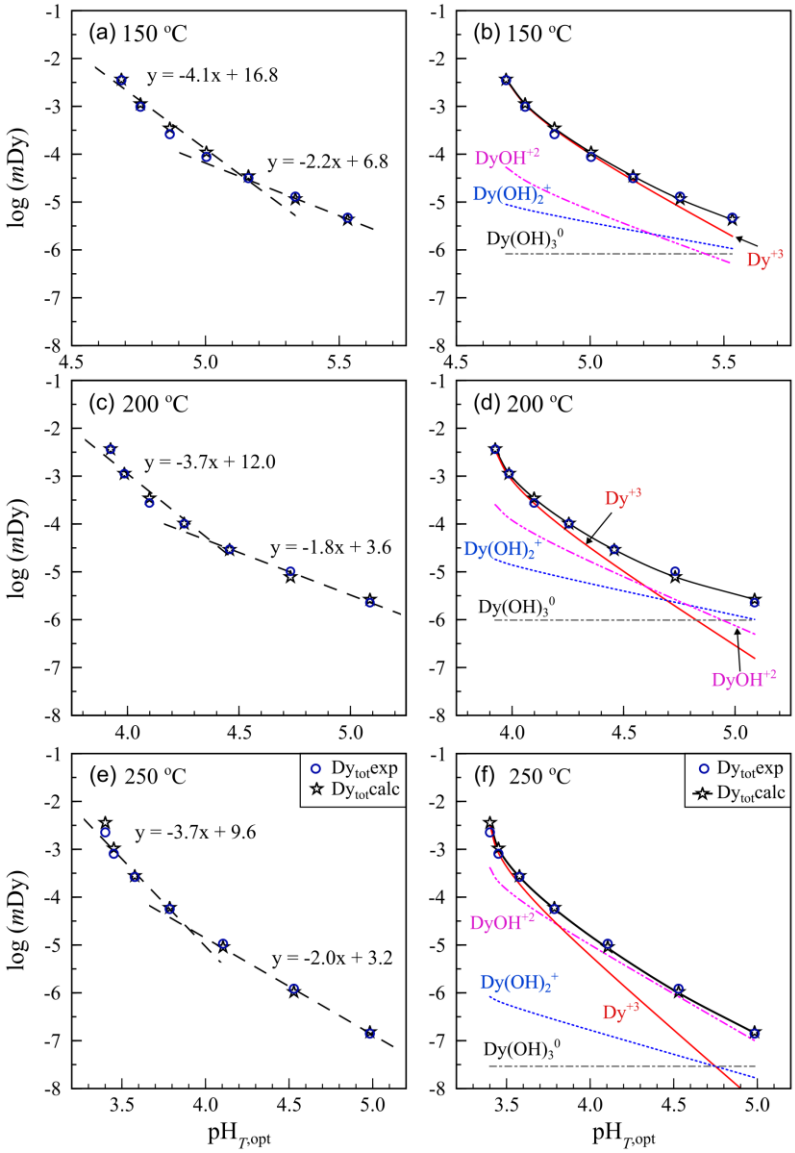

758

759 **Figure 6.** Dy solubility and Dy speciation as a function of optimized pH values (Table S4; $pH_{T,opt}$)
760 calculated at (a-b) 150 °C, (c-d) 200 °C, and (e-f) 250 °C using GEMS and the optimized $\Delta_f G°_T$
761 values for aqueous Dy species derived in this study (Table 3). Equations and dashed black lines in
762 (a), (c), (e) are from linear fits of the calculated Dy concentration (Dy_{tot}calc) and illustrate changes
763 to the slopes controlled by Dy^{3+} (lower pH range) and Dy hydroxyl complexes (higher pH range).

764

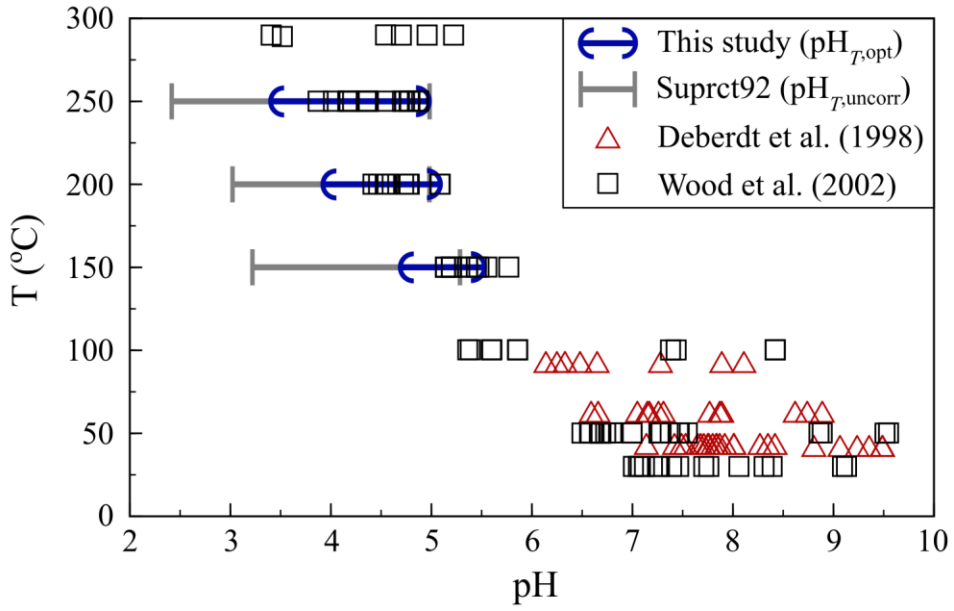

765

766 **Figure 7.** Comparison of the pH range predicted at the experimental conditions using the
767 optimized thermodynamic properties for aqueous Dy species derived in this study (Table 3; Table
768 S4, $pH_{T,opt}$) and from Supcrt92 (Table S3, $pH_{T,unorr.}$). For comparison, data are shown based on *in*
769 *situ* pH measurements for the solubility of $Nd(OH)_3$ by Wood et al. (2002) and for the solubility
770 of $La(OH)_3$ and Gd $(OH)_3$ by Deberdt et al. (1998).

771

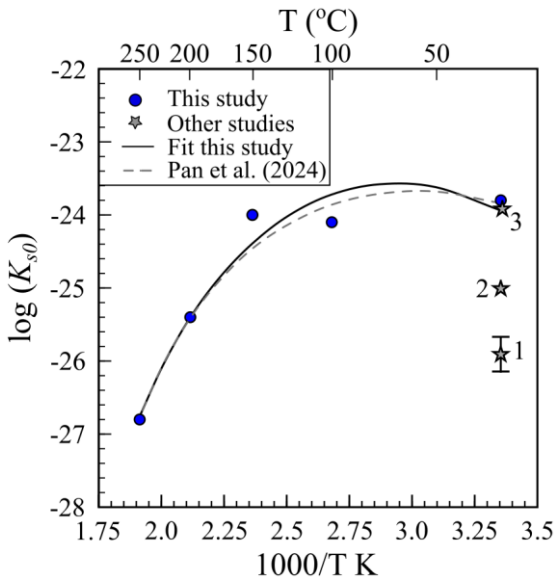

772

773 **Figure 8.** Comparison of the solubility constants logK_{s0} for Dy hydroxide as a function of inverse
774 temperature (1000/T in K) derived in this study between 25 and 250 °C and comparison to
775 available solubility data from the literature. The optimized logK_{s0} are calculated from
776 thermodynamic data for Dy^{3+} reported in Table 3 and the OH^- and Dy hydroxide from Table S2.
777 The regressed fits as a function of temperature are listed in Table 5. The dashed gray line represents
778 solubility products calculated from the 25 °C $\Delta_f G°$ value for the Dy^{3+} aqua ion derived from Pan
779 et al. (2024) combined with the HKF parameters from Haas et al. (1995). The stars represent
780 literature values at 20 and 25 °C: (1) Aksel'rud and Spivakovskii (1960); (2) Kovalenko et al.
781 (1966); (3) Orhanović et al. (1966). The error bars (or symbol sizes) represent the standard
782 deviation (1 σ) of data.

783

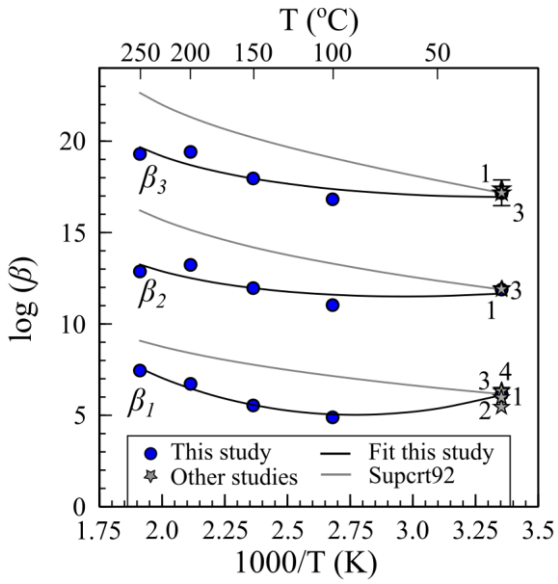

Figure 9. Comparison of the logarithm of formation constants (β_1-β_3) (Eqs. 4-6) for the hydrolysis of Dy^{3+} as a function of inverse temperature (1000/T in K) derived in this study (Table 5) between 25 and 250 °C and comparison to available formation constants from the literature and predicted values from Supcrt92 (Table S2 and S7). The stars indicate literature values: (1) Compilation by Baes and Mesmer (1976); (2) Luo et al., (1990); (3) Lee and Bryne (1992); (4) Klungness and Bryne (2000). The error bars (or symbol sizes) represent the standard deviation (1 σ) of data.

Supplementary materials

Hydrothermal solubility of Dy hydroxide as a function of pH and stability of Dy hydroxyl aqueous complexes from 25 to 250 °C

Sarah E. Smith-Schmitz [a,*], Alexander P. Gysi [a,b]

[a] New Mexico Bureau of Geology and Mineral Resources, New Mexico Institute of Mining and Technology, Socorro, NM 87801, USA

[b] Department of Earth and Environment Science, New Mexico Institute of Mining and Technology, Socorro, NM 87801, USA

[*] Corresponding author: Email address: sarah.smith@nmt.edu

Table S1. Summary of main Raman modes from analyses of pre- and post- experimental Dy hydroxide solids used in this study measured using 532 nm excitation laser.

Raman shift (cm^{-1})				Vibrational modes[a]
$Dy(OH)_3$(*s*) synthesized	Post experiment 150 °C	Post experiment 200 °C	Post experiment 250 °C	
132	132	132	133	
313	313	313	313	A_g or A_{1g}
396	397	397	395	A_g or E_{2g}
407	408	409	406	A_g
502	502	502	502	E_{1g}
3598	3597	3597	3598	*ν*OH
3612	3611	3611	3612	*ν*OH

[a] Vibrational mode assignments based on Arunachalam et al. (2018), Sanivarapu et al. (2018), and Hurtig et al. (2024)

Table S2. Thermodynamic data for solids and aqueous species included in calculations of $Dy(OH)_3$(s) solubility, aqueous Dy speciation, and as initial values for the optimization calculations. $C_P° = a_0 + a_1 \cdot T + a_2 \cdot T^{-2} + a_3 \cdot T^{-1}$.

Solids	$\Delta_f G°$	$\Delta_f H°$	$S°$	$V°$	$C_P°$	a_0	$a_1 \times 10^4$	$a_2 \times 10^{-3}$	$a_3 \times 10^{-2}$				Refs
	(J·mol^{-1})	(J·mol^{-1})	(J·K^{-1}·mol^{-1})	(J·bar^{-1})	(J·K^{-1}·mol^{-1})	(J·K^{-1}·mol^{-1})	(J·K^{-2}·mol^{-1})	(J·K·mol^{-1})	(J·mol^{-1})				
$Dy(OH)_3$(*s*)	-1,294,800	-1,428,400	130.3	3.5493	114.05	174.60	122.88	1,137.2	-229.6				1
Dy_2O_3	-1,771,735	-1,863,400	149.8	4.2680	116.27	121.23	152.76	-845.8	0				2,3
Aqueous species	$\Delta_f G°$	$\Delta_f H°$	$S°$	$V°$	$C_p°$	a_1	a_2	a_3	a_4	c_1	c_2	w_0	
	(J·mol^{-1})	(J·mol^{-1})	(J·K^{-1}·mol^{-1})	(J·bar^{-1})	(J·K^{-1}·mol^{-1})	(cal·bar^{-1} ·mol^{-1})	(cal·mol^{-1})	(cal·K ·bar^{-1}·mol^{-1})	(cal·K ·mol^{-1})	(cal·K^{-1} ·mol^{-1})	(cal·K ·mol^{-1})	(cal·mol^{-1})	
Dy^{3+}	-664,001	-696,711	-231.0	-4.1428	-131.61	-0.30003	-1,510.74	11.6879	-21,545	9.5076	-99,419	237,920	5,6
$DyOH^{2+}$	-856,465	-903,493	-45.6	0.2827	-103.24	0.26154	-139.41	6.2950	-27,213	2.8769	-80,863	122,060	4
DyO^+	-809,186	-836,884	19.3	0.5453	-276.36	0.26935	-120.56	6.2255	-27,291	-28.1511	-164,991	47,990	4
DyO_2H^0	-996,629	-1,050,602	163.6	2.151	-473.22	0.46969	368.55	4.3051	-29,313	-60.3933	-260,730	-3,000	4
DyO_2^-	-947,258	-1,014,536	119.7	1.8435	-390.27	0.47414	379.36	4.2636	-29,357	-37.5629	-220,601	119,490	4
ClO_4^-	-8,535	-129,327	182.0	4.3904	-24.00	0.81411	1,556.54	-7.8077	-34,224	16.4500	-65,700	96,990	5
OH^-	-157,297	-230,024	-10.7	-0.4708	-136.34	0.12527	7.38	1.8423	-27,821	4.15000	-103,460	172,460	6
H^+	0	0	0	0	0	0	0	0	0	0	0	-	6
H_2O^0	-237183	-285881	69.9	1.8068	75.36	-	-	-	-	-	-	-	7

[1] Diakonov et al. (1998), C_p estimated from the data for $Tb(OH)_3$; [2] Morss and Konings (2004); [3] Konings et al. (2014) C_p data; [4] Haas et al. (1995); [5] Shock et al. (1997); [6] Shock and Helgeson (1988); [7] IAPS-84 equation-of-state (Kestin et al., 1984).

Table S3. Summary of initial pH ($pH_{init,25°C}$) of the perchloric acid based buffer solutions, calculated uncorrected pH ($pH_{T,uncorr}$) at temperature T and logarithm molality (mol/kg) of aqueous Dy species determined from the compositions of the quenched experimental solutions (Table 2). The calculations were conducted using GEMS and the thermodynamic data from Supcrt92 (Table S2). The listed values are averages and standard deviations (1σ) determined from replicate experiments.

T (°C)	$pH_{init,25°C}$	$pH_{T,uncorr}$	σ	$\log(m Dy^{3+})$ (mol/kg)	σ	$\log(m DyOH^{2+})$ (mol/kg)	σ	$\log(m Dy(OH)_2^{+})$ (mol/kg)	σ	$\log(m Dy(OH)_3^{0})$ (mol/kg)	σ	$\log(m Dy(OH)_4^{-})$ (mol/kg)	σ
150	2.00	3.2	0.08	-2.49	0.00	-3.51	0.08	-5.72	0.17	-8.21	0.25	-11.51	0.33
150	2.50	3.3	0.13	-3.08	0.01	-3.86	0.14	-5.89	0.26	-8.27	0.39	-11.53	0.52
150	3.00	3.5	0.08	-3.71	0.01	-4.18	0.08	-5.93	0.15	-8.07	0.22	-11.13	0.29
150	3.50	4.0	0.12	-4.40	0.00	-4.35	0.12	-5.61	0.24	-7.27	0.36	-9.89	0.48
150	4.00	4.5	0.04	-5.22	0.01	-4.70	0.03	-5.44	0.07	-6.64	0.11	-8.79	0.15
150	4.50	5.0	0.09	-6.21	0.05	-5.14	0.05	-5.40	0.14	-6.09	0.24	-7.76	0.34
150	5.00	5.3	0.01	-7.21	0.01	-5.78	0.01	-5.69	0.02	-6.03	0.04	-7.35	0.05
200	2.00	3.0	0.03	-2.61	0.00	-2.94	0.03	-4.76	0.06	-6.95	0.09	-9.96	0.12
200	2.50	3.2	0.02	-3.31	0.00	-3.21	0.01	-4.67	0.03	-6.57	0.04	-9.37	0.06
200	3.00	3.4	0.01	-4.11	0.00	-3.73	0.01	-4.96	0.02	-6.68	0.04	-9.34	0.05
200	3.50	3.9	0.03	-5.06	0.01	-4.12	0.02	-4.80	0.06	-6.01	0.09	-8.18	0.13
200	4.00	4.3	0.02	-6.09	0.00	-4.74	0.02	-5.03	0.03	-5.86	0.05	-7.66	0.06
200	4.50	4.7	0.03	-7.25	0.01	-5.46	0.04	-5.32	0.07	-5.73	0.10	-8.11	0.14
200	5.00	5.0	0.01	-8.64	0.02	-6.49	0.03	-6.00	0.03	-6.06	0.03	-7.10	0.04
250	2.00	2.4	0.09	-3.87	0.05	-3.05	0.13	-4.99	0.22	-7.44	0.31	-10.67	0.41
250	2.50	2.9	0.05	-3.93	0.01	-3.34	0.06	-4.60	0.10	-6.46	0.15	-9.19	0.20
250	3.00	3.3	0.06	-4.74	0.01	-3.67	0.08	-4.48	0.14	-5.94	0.20	-8.30	0.27
250	3.50	3.7	0.03	-5.90	0.04	-4.41	0.07	-4.83	0.10	-5.92	0.14	-7.95	0.17
250	4.00	4.1	0.01	-7.26	0.06	-5.33	0.07	-5.32	0.09	-6.00	0.10	-7.63	0.11
250	4.50	4.5	0.00	-9.07	0.05	-6.67	0.05	-6.21	0.06	-6.44	0.06	-7.64	0.06
250	5.00	5.0	0.00	-11.15	0.05	-8.28	0.05	-7.34	0.05	-7.11	0.05	-7.85	0.05

Table S4. Aqueous speciation calculations using GEMFITS, the compositions of the quenched experimental solutions (Table 2) and the optimized Dy species properties from Table 3. Listed are the optimized pH values at temperature T ($pH_{T,opt}$), the measured and calculated total dissolved Dy molalities (mDy), and the aqueous Dy species molalities for experimental solutions equilibrated with Dy hydroxide solids at temperatures of 150, 200, and 250 °C at saturated water vapor pressure.

Experiment	T (°C)	log(mDy) meas (mol/kg)	log(mDy) calc (mol/kg)	residual %	$pH_{T,opt}$	log($m Dy^{3+}$) (mol/kg)	log($m DyOH^{2+}$) (mol/kg)	log($m Dy(OH)_2^{+}$) (mol/kg)	log($m Dy(OH)_3^0$) (mol/kg)
DyPO4-1[a]	100	-6.25	-6.29	-0.61	2.03	-6.29	-11.9	-	-
DyPO4-2[a]	100	-6.25	-6.27	-0.19	2.03	-6.27	-11.9	-	-
DyPO4-3[a]	100	-6.21	-6.16	0.79	2.02	-6.16	-11.8	-	-
DyOH-sol-150-2A	150	-2.46	-2.44	0.76	4.69	-2.44	-4.27	-5.05	-6.08
DyOH-sol-150-2B	150	-2.44	-2.44	0.30	4.69	-2.44	-4.27	-5.05	-6.08
DyOH-sol-150-2C	150	-2.46	-2.44	0.90	4.69	-2.44	-4.27	-5.05	-6.08
DyOH-sol-150-2.5A	150	-3.01	-2.95	2.11	4.76	-2.96	-4.55	-5.15	-6.08
DyOH-sol-150-2.5B	150	-3.04	-2.95	2.87	4.76	-2.96	-4.55	-5.15	-6.08
DyOH-sol-150-2.5C	150	-2.98	-2.95	0.95	4.76	-2.96	-4.55	-5.15	-6.08
DyOH-sol-150-3F	150	-3.61	-3.46	4.11	4.87	-3.48	-4.85	-5.28	-6.08
DyOH-sol-150-3G	150	-3.53	-3.46	2.18	4.87	-3.48	-4.85	-5.28	-6.08
DyOH-sol-150-3H	150	-3.60	-3.46	3.94	4.87	-3.48	-4.85	-5.28	-6.08
DyOH-sol-150-3I	150	-3.59	-3.46	3.61	4.87	-3.48	-4.85	-5.28	-6.08
DyOH-sol-150-3.5A	150	-4.11	-3.96	3.61	5.00	-4.01	-5.18	-5.43	-6.08
DyOH-sol-150-3.5B	150	-4.08	-3.96	3.04	5.00	-4.01	-5.18	-5.43	-6.08
DyOH-sol-150-3.5C	150	-3.98	-3.96	0.44	5.00	-4.01	-5.18	-5.43	-6.08
DyOH-sol-150-4A	150	-4.53	-4.46	1.65	5.16	-4.54	-5.52	-5.60	-6.08
DyOH-sol-150-4B	150	-4.49	-4.46	0.84	5.16	-4.54	-5.52	-5.60	-6.08
DyOH-sol-150-4C	150	-4.48	-4.46	0.45	5.16	-4.54	-5.52	-5.60	-6.08
DyOH-sol-150-4.5A	150	-4.96	-4.94	0.59	5.34	-5.11	-5.89	-5.77	-6.08
DyOH-sol-150-4.5B	150	-4.82	-4.94	-2.49	5.34	-5.11	-5.89	-5.77	-6.08
DyOH-sol-150-4.5C	150	-4.88	-4.94	-1.13	5.34	-5.11	-5.89	-5.77	-6.08
DyOH-sol-150-5A	150	-5.34	-5.36	-0.42	5.53	-5.71	-6.29	-5.97	-6.08
DyOH-sol-150-5B	150	-5.30	-5.36	-1.11	5.53	-5.71	-6.29	-5.97	-6.08
DyOH-sol-150-5C	150	-5.34	-5.36	-0.48	5.53	-5.71	-6.29	-5.97	-6.08
DyPO4-4[a]	150	-6.37	-6.34	0.60	2.03	-6.34	-10.7	-	-
DyPO4-5[a]	150	-6.31	-6.32	-0.24	2.03	-6.32	-10.7	-	-

Table S4. (Continued)

Experiment	T (°C)	log(mDy) meas (mol/kg)	log(mDy) calc (mol/kg)	residual %	$pH_{T,opt}$	log($m Dy^{3+}$) (mol/kg)	log($m DyOH^{2+}$) (mol/kg)	log($m Dy(OH)_2^{+}$) (mol/kg)	log($mDy(OH)_3^0$) (mol/kg)
DyOH-sol-200-2A	200	-2.44	-2.43	0.41	3.92	-2.47	-3.60	-4.74	-6.01
DyOH-sol-200-2B	200	-2.43	-2.43	0.02	3.92	-2.47	-3.60	-4.74	-6.01
DyOH-sol-200-2.5A	200	-2.95	-2.95	0.21	3.99	-3.01	-3.88	-4.84	-6.01
DyOH-sol-200-2.5B	200	-2.94	-2.95	-0.06	3.99	-3.01	-3.88	-4.84	-6.01
DyOH-sol-200-3A	200	-3.56	-3.46	2.62	4.10	-3.57	-4.20	-4.98	-6.01
DyOH-sol-200-3B	200	-3.57	-3.46	2.98	4.10	-3.57	-4.20	-4.98	-6.01
DyOH-sol-200-3.5A	200	-3.97	-3.99	-0.34	4.25	-4.17	-4.57	-5.15	-6.01
DyOH-sol-200-3.5B	200	-4.01	-3.99	0.62	4.25	-4.17	-4.57	-5.15	-6.01
DyOH-sol-200-4A	200	-4.51	-4.54	-0.50	4.46	-4.86	-5.01	-5.36	-6.01
DyOH-sol-200-4B	200	-4.55	-4.54	0.18	4.46	-4.86	-5.01	-5.36	-6.01
DyOH-sol-200-4.5A	200	-5.04	-5.11	-1.33	4.73	-5.72	-5.58	-5.64	-6.01
DyOH-sol-200-4.5B	200	-4.94	-5.11	-3.34	4.73	-5.72	-5.58	-5.64	-6.01
DyOH-sol-200-5A	200	-5.67	-5.58	1.58	5.09	-6.81	-6.30	-6.00	-6.01
DyOH-sol-200-5B	200	-5.62	-5.58	0.80	5.09	-6.81	-6.30	-6.00	-6.01
DyPO4-6[a]	200	-7.38	-7.47	-1.29	2.03	-7.47	-10.4	-	-
DyPO4-7[a]	200	-7.49	-7.35	1.80	2.03	-7.35	-10.3	-	-
DyOH-sol-250-2D	250	-2.72	-2.44	10.10	3.40	-2.50	-3.39	-6.08	-7.53
DyOH-sol-250-2G	250	-2.69	-2.44	9.03	3.40	-2.50	-3.39	-6.08	-7.53
DyOH-sol-250-2E	250	-2.71	-2.44	9.95	3.40	-2.50	-3.39	-6.08	-7.53
DyOH-sol-250-2H	250	-2.55	-2.44	4.18	3.40	-2.50	-3.39	-6.08	-7.53
DyOH-sol-250-2I	250	-2.57	-2.44	4.80	3.40	-2.50	-3.39	-6.08	-7.53
DyOH-sol-250-2.5A	250	-3.16	-2.98	5.67	3.45	-3.08	-3.68	-6.18	-7.53
DyOH-sol-250-2.5B	250	-3.08	-2.98	3.18	3.45	-3.08	-3.68	-6.18	-7.53
DyOH-sol-250-2.5C	250	-3.09	-2.98	3.67	3.45	-3.08	-3.68	-6.18	-7.53
DyOH-sol-250-2.5D	250	-3.04	-2.98	2.11	3.45	-3.08	-3.68	-6.18	-7.53
DyOH-sol-250-3A	250	-3.70	-3.55	3.87	3.58	-3.72	-4.05	-6.33	-7.53
DyOH-sol-250-3B	250	-3.53	-3.55	-0.61	3.58	-3.72	-4.05	-6.33	-7.53
DyOH-sol-250-3C	250	-3.55	-3.55	-0.03	3.58	-3.72	-4.05	-6.33	-7.53
DyOH-sol-250-3D	250	-3.53	-3.55	-0.82	3.58	-3.72	-4.05	-6.33	-7.53

Table S4. (Continued)

Experiment	T (°C)	log(mDy) meas (mol/kg)	log(mDy) calc (mol/kg)	residual %	$pH_{T,opt}$	log($m Dy^{3+}$) (mol/kg)	log($m DyOH^{2+}$) (mol/kg)	log($m Dy(OH)_2^{+}$) (mol/kg)	log($mDy(OH)_3^0$) (mol/kg)
DyOH-sol-250-3.5A	250	-4.34	-4.22	2.80	3.79	-4.51	-4.54	-6.56	-7.53
DyOH-sol-250-3.5B	250	-4.29	-4.22	1.64	3.79	-4.51	-4.54	-6.56	-7.53
DyOH-sol-250-3.5C	250	-4.16	-4.22	-1.36	3.79	-4.51	-4.54	-6.56	-7.53
DyOH-sol-250-3.5D	250	-4.28	-4.22	1.51	3.79	-4.51	-4.54	-6.56	-7.53
DyOH-sol-250-3.5E	250	-4.16	-4.22	-1.36	3.79	-4.51	-4.54	-6.56	-7.53
DyOH-sol-250-4A	250	-5.09	-5.04	0.90	4.10	-5.55	-5.21	-6.89	-7.53
DyOH-sol-250-4B	250	-5.01	-5.04	-0.63	4.10	-5.55	-5.21	-6.89	-7.53
DyOH-sol-250-4C	250	-4.92	-5.04	-2.45	4.10	-5.55	-5.21	-6.89	-7.53
DyOH-sol-250-4D	250	-4.88	-5.04	-3.38	4.10	-5.55	-5.21	-6.89	-7.53
DyOH-sol-250-4E	250	-4.98	-5.04	-1.22	4.10	-5.55	-5.21	-6.89	-7.53
DyOH-sol-250-4.5B	250	-5.99	-5.98	0.14	4.53	-6.86	-6.08	-7.31	-7.53
DyOH-sol-250-4.5C	250	-5.86	-5.98	-2.06	4.53	-6.86	-6.08	-7.31	-7.53
DyOH-sol-250-4.5Dii	250	-5.92	-5.98	-0.96	4.53	-6.86	-6.08	-7.31	-7.53
DyOH-sol-250-4.5Eii	250	-5.89	-5.98	-1.59	4.53	-6.86	-6.08	-7.31	-7.53
DyOH-sol-250-5A	250	-6.82	-6.82	0.00	4.98	-8.25	-7.00	-7.77	-7.53
DyOH-sol-250-5B	250	-6.86	-6.82	0.55	4.98	-8.25	-7.00	-7.77	-7.53
DyOH-sol-250-5D	250	-6.82	-6.82	-0.02	4.98	-8.25	-7.00	-7.77	-7.53
DyOH-sol-250-5E	250	-6.92	-6.82	1.42	4.98	-8.25	-7.00	-7.77	-7.53
DyPO4-8[a]	250	-8.31	-8.23	0.93	2.05	-8.23	-10.3	-	-
DyPO4-9[a]	250	-8.26	-8.12	1.63	2.05	-8.13	-10.2	-	-

[a] Calculated using $DyPO_4$ solubility data from Gysi et al. (2015)

Table S5. Summary statistics of the optimization calculations presented in Table 3, indicating the composite scaled sensitivities (CSS) and the correlation factor (corr) between fitted Dy species.

	Optimized species	CSS	corr Dy^{3+}	corr $DyOH^{+2}$	corr DyO^{+a}
T=150 °C					
O	Dy^{+3}	6.1	-	0.0003	-
O	$DyOH^{+2}$	11.0	0.0003	-	-
R	DyO^{+a}	-	-	-	-
R	DyO_2H^{0b}	-	-	-	-
T=200 °C					
O	Dy^{+3}	6.5	-	0.0100	-0.0511
O	$DyOH^{+2}$	6.6	0.0100	-	-0.7451
O	DyO^{+}	11.0	-0.0511	-0.7451	-
R	DyO_2H^{0}	-	-	-	-
T=250 °C					
O	Dy^{+3}	8.0	-	-0.4550	0.2193
O	$DyOH^{+2}$	27.9	-0.4550	-	-0.6732
O	DyO^{+}	3.4	0.2193	-0.6732	-
R	DyO_2H^{0}	-	-	-	-

[a] Anhydrous species notation corresponding to $Dy(OH)_2^{+}$ calculated from $DyO^{+} + H_2O = Dy(OH)_2^{+}$.
[b] Anhydrous species notation corresponding to $Dy(OH)_3^{0}$ calculated from $DyO_2H^{0} + H_2O = Dy(OH)_3^{0}$.

Table S6. Compilation of the logarithm of Dy hydroxide solubility productions (K_{s0}) and Dy formation constants (β_1-β_3) reported in the literature.

T (°C)	log$K$	Reference
	(K_{s0})	
25	-25.9	Aksel'rud and Spivakovskii (1960)
20	-25.0	Kovalenko et al. (1966)
20	-23.8	Orhanović et al. (1966)
25	-28.02	Diakonov et al. (1998b)
	(β_1)	
25	6.0[a]	Baes and Mesmer (1976)
25	5.45[a]	Luo et al. (1990)
25	6.19[a]	Lee and Byrne (1992)
25	6.41[a]	Klungness and Byrne (2000)
40	6.34[a]	Klungness and Byrne (2000)
55	6.23[a]	Klungness and Byrne (2000)
	(β_2)	
25	11.8[a]	Baes and Mesmer (1976)
25	11.9[a]	Lee and Byrne (1992)
	(β_3)	
25	17.3[a]	Baes and Mesmer (1976)
25	17.16[a]	Lee and Byrne (1992)

[a] Formation constants re-calculated from reported hydrolysis constants and the thermodynamic properties listed in Table S2.

Table S7. Logarithm equilibrium constants calculated from 25 to 250 °C using regressed coefficients from Table 5 and the function $\log K = A_0 + A_1T + A_2/T + A_3\ln T + A_4/T^2$, with T in Kelvin. For comparison logarithm equilibrium constants calculated using thermodynamic parameters from Supcrt92 are also listed.

	This study				Supcrt92			
T (°C)	$\log K_{s0}$	$\log\beta_1$	$\log\beta_2$	$\log\beta_3$	$\log K_{s0}$	$\log\beta_1$	$\log\beta_2$	$\log\beta_3$
25	-23.94	6.10	11.66	16.94	-27.84	6.16	11.88	17.16
50	-23.62	5.36	11.52	17.01	-27.38	6.50	12.37	17.86
75	-23.58	5.06	11.51	17.17	-27.14	6.83	12.84	18.49
100	-23.72	5.05	11.60	17.38	-27.06	7.15	13.30	19.08
125	-24.00	5.24	11.75	17.65	-27.11	7.46	13.74	19.64
150	-24.39	5.57	11.96	17.95	-27.28	7.77	14.19	20.19
175	-24.86	5.98	12.21	18.30	-27.56	8.08	14.66	20.74
200	-25.41	6.47	12.51	18.69	-27.94	8.40	15.14	21.32
225	-26.05	7.00	12.85	19.14	-28.43	8.73	15.65	21.94
250	-26.77	7.58	13.25	19.67	-29.05	9.08	16.21	22.64

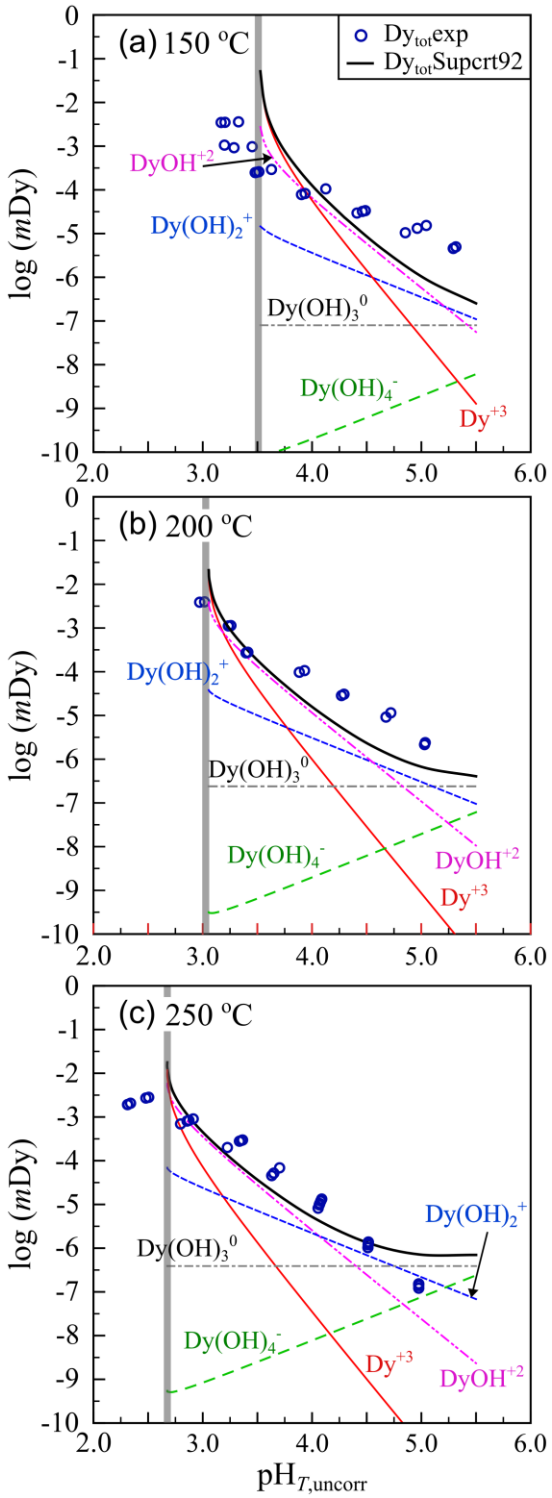

Fig. S1. Logarithm of total dissolved Dy concentrations (mol/kg) in the quenched experimental solutions versus uncorrected pH values calculated at temperature T ($pH_{T,uncorr}$) using the thermodynamic data from Supcrt92 (Table S2) for experiments conducted at (a) 150 °C, (b) 200 °C, and (c) 250 °C. For comparison, the calculated Dy solubility and Dy speciation is shown for perchloric acid based solutions in equilibrium with $Dy(OH)_3$(s) calculated using GEMS and the thermodynamic data listed in Table S2. The gray bars indicate the low pH solubility limit for $Dy(OH)_3$(s). The comparison indicates discrepancies between model and experimental data, and problems in calculated $pH_{T,uncorr}$ values, that can be resolved using the optimized thermodynamic data derived in this study (Table 3).

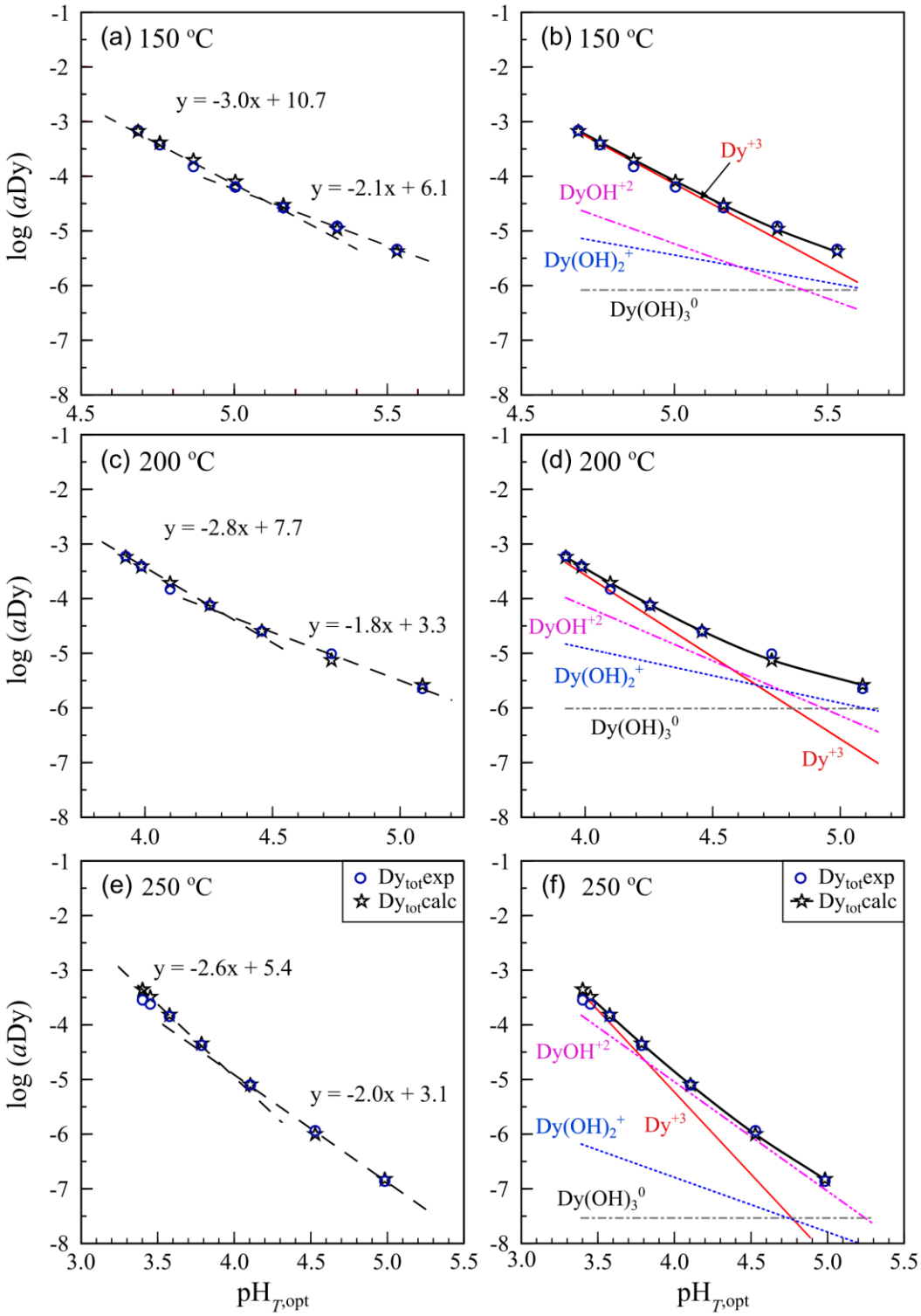

Fig. S2. Calculated activities of Dy species as a function of optimized pH values calculated at (a-b) 150 °C, (c-d) 200 °C, and (e-f) 250 °C using GEMS and the optimized $\Delta_f G°_T$ values for aqueous Dy species derived in this study (Table 3). The logarithm of the sum of the calculated activities of Dy species for the measured ($Dy_{tot}exp$) and calculated ($Dy_{tot}calc$) Dy concentrations in table S4 are shown. Equations and dashed black lines in (a), (c), (e) are from linear fits of the logarithm of the sum of the calculated activities and illustrate changes to the slopes due to changes in Dy speciation.

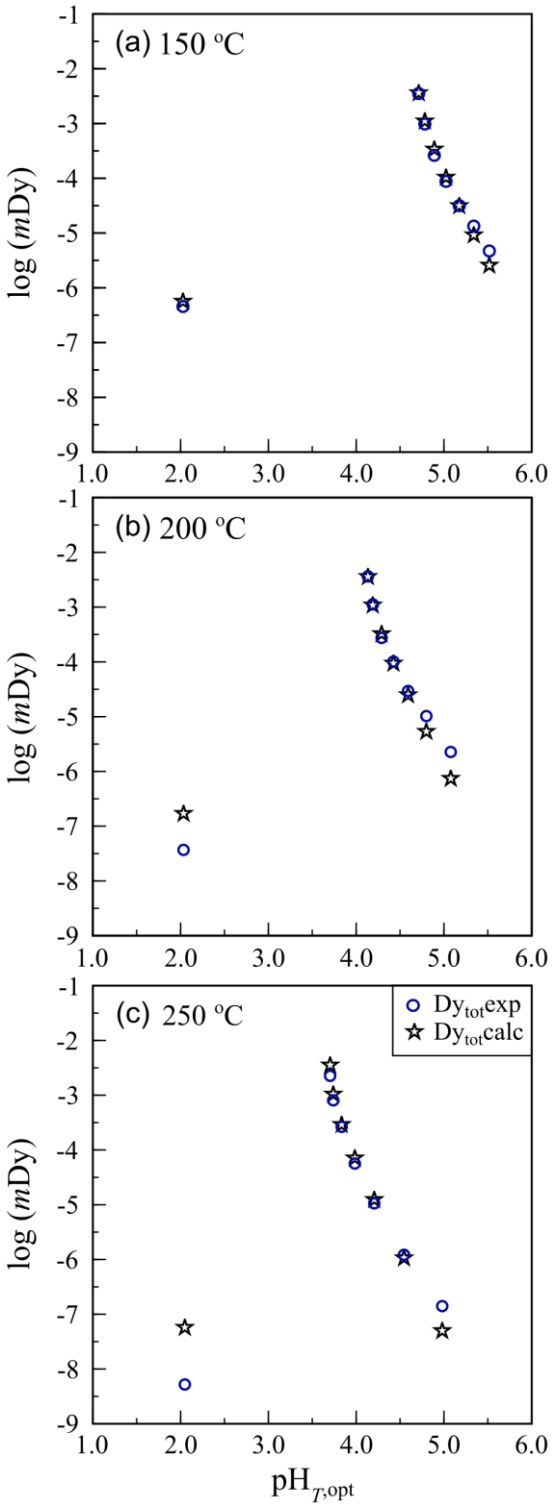

Figure S3. Test optimization calculations using GEMSFITS and the assumption that only Dy^{3+} controls speciation in the studied pH range at (a) 150 °C, (b) 200 °C, and (c) 200 °C. The plots show the modeled (stars) vs. the measured (circles) solubility data for Dy hydroxide derived in this study at pH >3 and $DyPO_4$ at pH of 2 with data from the study of Gysi et al. (2015). The mismatch between experimental data and optimizations indicates that Dy hydroxyl species should be included in the optimizations; if they are not, the solubility of $DyPO_4$ at pH of 2 is overestimated and the solubility of Dy hydroxide in the higher pH range of the experiments is underestimated with respect to the experimental data.